APPLICATION OF SIMULATION TECHNIQUES FOR MODELLING UNCERTAINTY ASSOCIATED WITH GOLD MINERALISATION

Yelena Michailovna van der Grijp

A project report submitted to the Faculty of Engineering and the Built Environment, University of the Witwatersrand, in partial fulfilment of the requirements for the degree of Master of Science in Engineering by advanced coursework and research

Johannesburg, 2014

DECLARATION

I declare that this project is my own unaided work. It is being submitted for the degree of Master of Science in Engineering in the University of Witwatersrand, Johannesburg. A part of the research report relating to practical application of the methodology is concurrently being submitted for a Certificate of completing a Citation Programme in Applied Geostatistics at the University of Alberta, Edmonton.

The information used in the thesis has been obtained by me while being employed by AngloGold Ashanti.

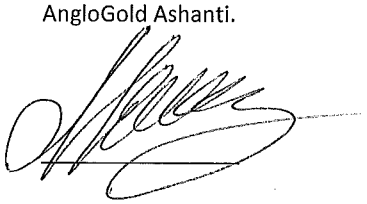

16 day of May 2014

ABSTRACT

The current research investigates applicability of stochastic approach to simulation of gold distribution to assess uncertainty of the associated mineralisation and proposes a practical workflow to be used in future for similar problems. Two different techniques are explored in the research: Direct Sampling multi-point simulation algorithm is used for generating realisations of lithologies hosting the gold mineralisation, Sequential Gaussian Simulation is applied to generate multiple realisations of gold within them. A number of parameters in the Direct Sampling algorithm are investigated to arrive at good reproducibility of the patterns found in the training image. The findings arrived at are aimed to help when undertaking simulation in future and choosing appropriate parameters. The resulting realisations are analysed for assessment of combined uncertainty in the lithology and gold mineralisation. Different assessment criteria are demonstrated to visualise and analyse uncertainty. Block scaling to a panel size resolution is carried out to compare the results of the stochastic modelling to a kriged model and assess global uncertainty which stems from this analysis. A practical workflow has been reached as a result of the research.

The approach confirms usefulness of the simulation in the estimation of uncertainty and provides some practical considerations in usage of Direct Sampling method which can be applied to other MPS algorithms with further improvements.

ACKNOWLEDGEMENTS

I would like to thank a number of people without whom this work would not be possible:

Professor Clayton Deutsch, for his inspirational and invigorating lectures;

The staff at the University of Neuchâtel, namely Professor Philippe Renard and Dr. Julien Straubhaar, for providing support in usage of the Direct Sampling code;

Professor Richard Minnitt, for his support in entering into an agreement with the University of Neuchâtel on my behalf for utilisation of the Direct Sampling algorithm as an essential element of the workflow used in the research;

Management at AngloGold Ashanti, for providing data, sponsorship and the most luxurious commodity in the modern days – time to carry out this project;

My parents, for everything they gave me;

My husband, Bennett. Without his love and eternal support this work would not have been possible;

My son, Henri, for his patience and humour when most needed.

CONTENTS

DECLARATION ..... **iii**

ABSTRACT ..... **iv**

ACKNOWLEDGEMENTS ..... **v**

LIST OF FIGURES ..... **viii**

LIST OF TABLES ..... **ix**

LIST OF SYMBOLS ..... **x**

PHYSICAL QUANTITIES ..... **x**

NOMENCLATURE ..... **x**

1. INTRODUCTION **1**

1.1 Uncertainty modelling: 2-point versus multi-point statistics **1**

1.2 Sequential simulation algorithm **3**

1.3 History overview **4**

1.4 Research motivation **5**

1.5 Research methods **5**

1.6 Project report structure **6**

2 SUMMARY OF METHODOLOGY **7**

2.1 Lithology simulation **7**

2.1.1 Description of the Direct Sampling algorithm to perform multi-point simulation 7

2.1.2 Input into the Direct Sampling algorithm 8

2.2 Simulation of grade **10**

3 PRACTICAL APPLICATION OF THE SIMULATION ALGORITHMS **12**

3.1 Geological settings **12**

3.2 Data description **13**

3.3 Conventions used in the report **13**

3.4 Training image **14**

3.4.1 TI statistics 16

3.4.2 TI variography 17

3.4.3 Validating a training image 19

3.5 Simulation of the main area 23
3.5.1 Lithology simulation 23
3.5.2 Grade simulation 29
3.6 Discussion 32

4 POST-PROCESSING FOR UNCERTAINTY 36
4.1 Visualising uncertainty 36
4.1.1 Post-processing lithology 36
4.1.2 Post-processing grade 37
4.2 Block averaging to recoverable resources 40
4.3 Comparison to a kriged model 41
4.4 Discussion 45

5 CONCLUSION AND RECOMMENDATIONS 47
5.1 Summary of findings 47
5.2 Recommendations for a future use of an MPS approach 48
5.3 General recommendations on stochastic modelling workflow 48
5.4 Recommendations for future work 48

6 REFERENCES 50

7 APPENDICES 52
Appendix A: Variograms of the conditioning drillhole samples within the training image 52
Appendix B: Variograms of the Sequential Gaussian Simulation results within the training image 59

LIST OF FIGURES

Figure 3.1. Isoclinal view of the Nyankanga pit showing drillholes dataset used in the simulation. 13
Figure 3.2. Legends used in the graphics of the report 14
Figure 3.3. Drillholes used in the creation of a training image. 14
Figure 3.4. Wireframe model used to create a training image. 15
Figure 3.5. The three main lithologies in the training image. 15
Figure 3.6. Au statistics of the conditioning data in the training image for the main lithology types. 16
Figure 3.7. Plan view of the study area showing the primary direction of continuity. 17
Figure 3.8. Unconditional simulation of lithology, sectional view. 20
Figure 3.9. Conditional simulation within the volume of the training image, sectional view of two realisations. 20
Figure 3.10. Histogram reproduction within the training image 21
Figure 3.11. Variogram reproduction for the simulated lithologies (BIF and diorite). 22
Figure 3.12. Conditional simulation of lithology over main grid, sectional and isoclinal views. 24
Figure 3.13. Conditional simulation of lithology over main grid, dykes conditioned by an additional grid object. 24
Figure 3.14. Second training image over the extent of the simulation volume, containing large-scale morphology of the dykes, sectional view. 25
Figure 3.15. Lithology simulation using 2 training images. 25
Figure 3.16. Dykes logging in the drillholes, isoclinal view. 26
Figure 3.17. Four realisations of lithology from the final simulation run, sectional view. 26
Figure 3.18. Histograms of the simulated lithology proportions across the 50 realisations. 27
Figure 3.19. Variogram validation for the 50 lithology realisations. 28
Figure 3.20. Four realisations of gold grade, sectional view. 30
Figure 3.21. Histograms of the simulated gold values vs conditioning data. 31
Figure 3.22. Variograms of the simulated gold realisations of BIF for the three principal directions of continuity. 31
Figure 3.23. Variograms of the simulated gold realisations of diorite for the three principal directions of continuity. 32
Figure 4.1. Summary of the post-processing output of lithology simulation. 36
Figure 4.2. Entropy for lithology simulations. 37
Figure 4.3. Post-processing results of the E-type averaging of the gold simulation, sectional view. 37
Figure 4.4. Post processing for a selected cut-off grade, sectional view. 38
Figure 4.5. Post-processing results of probability of being within 15% error of the Au E-type mean, sectional view. 38

Figure 4.6. Probability of being above a specified cut-off grade. 39
Figure 4.7. Plan view of the Nyankanga deposit showing the simulation grid with the drillhole samples. 39
Figure 4.8. An upscaled simulated model: probability of being within 15% error of the Au E-type mean, sectional view. 41
Figure 4.9. Deterministically interpreted volume of the ore along the shear zone used for comparison of the kriged model and simulation results. 42
Figure 4.10. Histograms of the kriged and simulated E-type average of gold at panel size blocks, compared within a common volume. 42
Figure 4.11. Comparison of the kriged and simulated gold grade for the cells falling within the shear zone. 43
Figure 4.12. Histograms of the densities assigned to the kriged model and simulated realisations, compared within a common volume. 43
Figure 4.13. Comparison of the densities in the kriged and simulated model cells falling within the shear zone. 44
Figure 4.14. Scatterplots of gold and density for simulated vs kriged model. 44

LIST OF TABLES

Table 3.1. Training image geometry 14
Table 3.2. Anisotropy directions 18
Table 3.3. Variogram model parameters for BIF/diorite interface 18
Table 3.4. Variogram model parameters for gold in original space 18
Table 3.5. Variogram model parameters for gold in Gaussian space 18
Table 3.6. Global proportions of the conditionally simulated lithologies within the training image 21
Table 3.7. Geometry of the main simulation grid 23
Table 3.8. Comparison of the simulated and input global lithology proportions 27

LIST OF SYMBOLS

$Z(u)$	Generic random variable at location u
$n(u)$	n conditioning data found in a neighbourhood centred at u

PHYSICAL QUANTITIES

g/cm^3	density, grams per cubic centimetre
g/t	metal concentration, grams per metric ton

NOMENCLATURE

3D	Three dimensional
Au	Gold
BIF	Banded iron formation
cdf	Cumulative distribution function
DC	Diamond core
DI	Diorite
E-type	Conditional expectation estimate obtained by point-wise averaging of simulated realisations
GSLIB	Geostatistical software library (Deutsch, 1998)
KLD	Kullback-Leibler divergence
mp	Multi-point
MPS	Multi-point statistics
pdf	Probability density function
QP	Quartz porphyry
RBF	Radial Basis Function
RC	Reverse circulation
SGS	Sequential Gaussian Simulation
TI	Training image

"As far as the laws of mathematics refer to reality, they are not certain;
and as far as they are certain, they do not refer to reality."
Albert Einstein

January 27, 1921

1. INTRODUCTION

1.1 Uncertainty modelling: 2-point versus multi-point statistics

Traditionally, modelling in mining industry is done in a deterministic way when only one representation of reality is considered. It is applicable to modelling stationary geological domains and mineral grade distribution within them. The main problem with deterministic models is that they convey a presumably perfect knowledge with regards to the size and geometry of the geological units and spatial continuity. This is a good approach if the density of the available data allows inferring the latter with high confidence. Problems arise when an interpretation is not definite and multiple scenarios can be inferred with equal validity from usually broadly spaced informing data (Perez, 2011).

In the last two decades there have been considerable advances in using uncertainty for mineral resource and reservoir assessment. The approach requires generating and summarising multiple stochastic models of the truth and has been mainly used in hydrogeology and oil industry. The methodology has not been broadly utilised in the mining industry due to a number of issues. The main one of them is a necessity to deal with large datasets and high demands in terms of processing power and technical expertise for generating geological and geostatistical models. These models must be further subjected to mine design and optimisation algorithms (Perez, 2011).

In the heart of the stochastic approach to modelling lies geostatistical simulation. When applied to modelling geology or grade distribution, the process serves as a platform for generating multiple scenarios. During the workflow, a number of equally probable models are created, each one of them providing a plausible version of a geostatistical reality. Analysing the suite of them all together allows assessment of uncertainty.

For this research, two approaches to stochastic modelling are applied: multi-point statistical simulation – for modelling geostatistical lithological domains, and subsequent to this, a Sequential Gaussian Simulation – for creating multiple realisations of the grade distribution within the simulated lithologies.

Traditional stochastic simulation techniques carry a heavy reliance on an input parametric model of spatial continuity. This approach, broadly described in the literature, is termed 2-point geostatistics (Remy, 2009). It has brought insights into geosciences by accounting for spatial relationships of data values. It consists of dividing a particular dataset into single locations of variables. The locations with known data values are considered in pairs to create a parametric description of spatial continuity. Each single data variable location is related then to a single location of unknown using the previously defined parametric model through the process of kriging to produce an estimate. This approach is very robust in generating the "best linear unbiased estimate". It can be used with different variations for estimating both continuous and categorical variables. However, it fails at reproducing complex non-linear geological shapes. The variogram analysis is not always easy since data can be noisy, there are errors in the data, there is not enough data or the data is too broadly spaced to capture the true variability. Variograms are crude descriptions of actual phenomena, since they capture spatial continuity by considering sample values taken only two at a time. The three parameters (nugget, range and sill) cannot describe a deposit that may need hundreds of parameters for a complete description (Caers, 2011).

A concept of multiple-point statistics (MPS) was first introduced by Guardiano and Srivastava in 1993. Its basic concept lies in a training image (TI) which conveys a conceptual model of geological heterogeneity on which further MPS simulation is based (Caers, 2011). An MPS approach is a relatively new tool for geostatisticians to communicate the spatial continuity style.

The multi-point simulation algorithm bypasses pair-wise division of the locations with the known data values. It uses an explicit multi-point model, which allows considering all n known data points together. The latter is termed "data conditioning". The necessary multi-point statistics are obtained from replicates of the conditioning data event found in a visually explicit training image. A training image is a conceptual representation of how z values of a random variable are jointly distributed in space, be it a continuous or a categorical variable. A TI is essentially an unconditional realisation of a random function model $Z(u)$. This model does not have to honour the data values at their spatial location. This "data conditioning" takes place during a further multi-point simulation. While a 2-point simulation aims at generating realisations that honour the data and the variogram model, a multi-point simulation generates realisations that honour the data and the multi-point structures present in the training image (Remy, 2009).

A training image represents complex curvi-linear structures involving more than two locations in space simultaneously. It needs to reflect only fundamental rules of the conceptual geological relationship in the study area. It does not have to be constrained to any specific data. The aim is to build realisations that mimic the spatial continuity of the training image, and at the same time constrain the model to the available sampling data. During the simulation a particular pattern present in the training image is randomised over the area being modelled (Caers, 2011).

Traditional geostatistics requires a variogram model for kriging. In many applications involving subsurface deposits where local data are sparse, inference of a variogram is difficult. In this case, a variogram can be borrowed from other deposits which are analogous to the one under study. It can also be modelled subjectively to reflect the geologist's appreciation of the spatial continuity. The MPS approach in this case is more intuitive for geologists. It is easier to adopt a geological section, a sketch, series of trench sections or an outcrop photograph as a training image representing the variability rather than to infer a variogram. In the case of a training image, stationarity is a modelling decision. Such a decision is largely subjective. It can only be tested by evaluating the success of the resulting model in achieving the task at hand. Accepting a spatial variogram model or accepting a specific training image amounts to different decisions on stationarity. The use of different training images allows interpretation of spatial geological information to be taken far beyond the variograms of these training images (Remy, 2009).

A word of warning is that the results of such multi-point geostatistical application are only as good as the prior model adopted using the training image. While the MPS approach attempts to provide solutions from a more realistic perspective, it requires a thorough understanding and interpretation of the geological phenomenon. Such interpretation is subject to a great deal of uncertainty in itself (Caers, 2011).

1.2 Sequential simulation algorithm

The size of geostatistical models reaches millions of cells and prevents most of them from being practical in terms of processing time. One method that does not suffer from this limitation is sequential simulation. The approach is to build a model one cell at a time and assign values to each cell by visiting each one along a random path, until all cells are visited. The value assigned to a cell depends on the values assigned to all previously visited cells along the random path. This sequential dependence forces a specific pattern of spatial continuity into a model. Each final result is termed a realisation. At each grid cell in a realisation, the probability of having a certain category or content of interest, given the previously simulated categories is calculated.

Sample data provide local constraints for the assigned values. During simulation, the grid cells closest to the data points are assigned values from the samples. These cells' values are "frozen". The cells containing such constraints are never visited again and their values are never re-considered. The sequential nature of the algorithm forces all neighbouring simulated cell values to be consistent with the data. Sequential simulation allows for constraint to data points in a single pass over all grid cells, no iteration is required (Caers, 2011).

In MPS, the conditional probability distribution is deduced directly from the training image. This probability depends on the spatial variation seen in the training image. In variogram-based

modelling, kriging is used to derive such probability distribution. This probability distribution needs to be conditioned to the data in both cases.

Unlike 2-point geostatistical algorithms, the MPS technique is only used in a simulation mode.

1.3 History overview

Monte Carlo experiments lay at the heart of the simulation algorithm lays. The modern version of it was invented as far back as the late 1940's by Stanislav Ulam for nuclear weapons projects. The algorithm relies on repeated random sampling to obtain numerical results. When Monte Carlo Simulations were applied in petroleum and space exploration, the resulting predictions of project failures, cost and time schedule overruns were recognised to be consistently better than human intuition or "soft" methods. There are three distinct problems where Monte Carlo methods are used: optimization, numerical integration and generation of samples from a probability distribution (http://en.wikipedia.org/wiki/Monte_Carlo_method). It has been used extensively since then.

With regards to the problem of optimisation of spatial phenomena, Deutsch and Journel introduced a theory of simulated annealing in 1992. In 1993, Guardiano and Srivastava introduced the concept of MPS for the first time. The theory of stochastic simulation was further advanced in 1994 by Caers with neural networks to collect MPS from training images. Further stepping stones included improvement in the theory of a single normal equation (Strebelle and Journel, 2000) and updating of conditional distributions with MPS by Ortiz and Deutsch in 2003 (Deutsch, 2013).

There have been a number of MPS algorithms developed in the last two decades, after the first introduction of the concept by Guardiano and Srivastava. In 2002, Strebelle proposed the *snesim* algorithm for simulation of categorical variables. It utilised a "search tree" structure to store conditional probabilities of data events which were extracted later during simulation. It was computationally demanding which made it prohibitive for simulation of large models. *Filtersim* algorithm (Zhang et al, 2006; Wu et al, 2008) accommodated both continuous and categorical variables, as well as improved the computational demands by simulating batches of pixels rather than one pixel at a time. *IMPALA* algorithm (Straubhaar et al, 2011) used lists instead of trees, which reduced the memory requirements by allowing parallelisation, however this was still demanding. In 2007, Arpat and Caers introduced *SIMPAT* algorithm which used distance functions to calculate similarity between the training image and conditioning data events. Multi-dimensional scaling, *MDS*, (Honarkhah and Caers, 2010) and *CCSIM* method (Tahmasebi et al, 2012) are other examples of the MPS algorithms (Rezaee, 2013).

1.4 Research motivation

The current research investigates the applicability of stochastic approach to the simulation of lithology and gold distribution to assess uncertainty of the associated mineralisation. An MPS algorithm is used to model spatial continuity of lithological units in a gold deposit, Sequential Gaussian Simulation (SGS) is applied subsequently to assess resulting uncertainty in gold distribution. There are many different MPS algorithms available currently which can be used successfully with sufficient proficiency. The purpose of the research is not to compare any of them, but rather to test the application of stochastic approach to a mining scenario, and demonstrate its plausibility in terms of time demands versus gains in generating a geostatistical model of uncertainty. Comparison of the averaged result of the simulation to a kriged model is performed. A workflow to be used in future for similar problems is proposed.

1.5 Research methods

The current work presents a case study of Nyankanga gold deposit, as an attempt to model and quantify uncertainty of different mineralised units. A suite of software was used for different parts of the project. The Direct Sampling (DS) algorithm developed recently at the University of Neuchâtel, was used to generate 50 realisations of lithology. The algorithm was operated on a Windows platform pc, from a command prompt.

A Sequential Gaussian Simulation framework was applied to simulate gold grades using Geostatistical Software Library (GSLIB) developed at the University of Stanford.

The lithology realisations were combined with the grade realisations to assess joint uncertainty in the interpretation of geostatistical domains and grade.

Preparation of the training image and visualisation was done using Leapfrog software. Most processing was done in GSLIB, Datamine software was used for some of the scripting.

The project was conducted with the gold values in the original units in order for the originators of the data to validate the results. Due to confidentiality reasons, no reference to actual gold values is made in the project report. Statistics which would allow one to infer the gold grades have been left out, where present – they have been modified.

The simulation algorithms were run on a solid-state 64-bit 8-core machine with 2.4GHz processor. All further references to processing time are with regards to this capacity.

1.6 Project report structure

Chapter 2 of the report provides an overview of the methodology employed to simulate lithologies and gold grade realisations. A detailed description of the practical workflow followed in the process is given in Chapter 3. The workflow explains the steps involved in creating a training image, the process followed for validating the workflow, the input parameters used in the simulation over the main volume of interest and difficulties encountered.

Chapter 4 covers some aspects of post-processing for uncertainty assessments. Block averaging to recoverable resources is touched on in this chapter, and comparison of global statistics for gold and rock density between the stochastic approach and a kriged model is presented.

In the last section, some recommendations stemming from the research and possible future work are suggested.

2 SUMMARY OF METHODOLOGY

Traditional practice in resource modelling is to generate a single smooth 3D model usually applying the ordinary kriging algorithm. Stochastic simulation on the other hand is used to generate multiple equi-probable realisations of a variable. While kriging variance does not account for uncertainty and the kriging estimates are overly smooth, the objective of the stochastic simulation is to model variability as a means for quantifying uncertainty in a natural phenomenon.

2.1 Lithology simulation

The lithology realisations were generated using the Direct Sampling (DS) algorithm supplied by the University of Neuchâtel, Switzerland.

2.1.1 Description of the Direct Sampling algorithm to perform multi-point simulation

The Direct Sampling algorithm is one of the recent multi-point simulation techniques. Similar to the other techniques, it adopts a principle of sequential simulation. The difference comes in the way of computing a conditional cumulative distribution function for the local data event. Rather than storing the training image probabilities in a catalogue prior to simulation, the algorithm directly scans and samples the training image in a random fashion while conditioning to the data event d_n. It uses dissimilarity distances between the d_n and TI patterns. For each node x in the simulation grid, the TI is randomly scanned for matching patterns of nodes denoted y. A measure of satisfying the degree of "matching" is determined by a user-defined distance threshold, which takes a range of values between 0 and 1. As soon as a TI pattern that matches the data event d_n exactly or within the defined threshold is found, the value of the central node of such TI pattern is pasted to x. The advantage of the DS over other MPS algorithms is that it by-passes the step of explicit calculation of the conditional cdf, and as a result many technical difficulties encountered in other algorithms are avoided. Since the TI is scanned randomly, this strategy is equal to drawing a random value from the cumulative distribution function, however the simulation speed is increased considerably (Mariethoz et al, 2013).

The DS algorithm can be applied to both categorical and continuous variables as well as to multivariate cases. Recently, a modified form of the algorithm was introduced, which allows

patch-pasting of groups of nodes at a time rather than a single-pixel pasting approach, combining the flexibility of DS with the processing efficiency of patch-based methods (Rezaee, 2013).

The detailed description of the DS algorithm, its parameters and their sensitivities, as well as practical considerations for different applications can be found in Mariethoz et al (2012, 2013).

2.1.2 Input into the Direct Sampling algorithm

As an input to the DS algorithm, a number of parameters need to be defined. A short description of the most important of them is provided below.

Simulation grid

A simulation grid represents the volume to be simulated. It is a Cartesian grid which is defined in terms of:

- Size, expressed in number of nodes in X, Y and Z directions;
- Node spacing in each direction;
- Coordinates of the origin cell (min X, min Y, min Z).

Training image

A training image is another type of a grid object, as such it is also described geometrically in terms of an origin, number of nodes in each direction and node spacing. Each node of the training image has at least one or a set of associated variables of interest. A training image does not have to be defined at each node, it can be defined partially. In this case, undefined cells carry a default value.

If required, a number of training images can be provided as an input to the algorithm. The simulation grid itself can serve as a training image. This can be useful when a portion of the simulation grid is well informed and the remaining part is to be reconstructed.

Conditioning data

The conditioning data can be in a form of a regularly gridded file, termed an “image file” or a point set file representing sample centroids. Multiple conditioning data files can be provided in the input.

Mask image

A mask image is a grid object with the same geometry as the simulation grid and flagging of 1 or 0 for nodes to be simulated or omitted from simulation. Providing a mask image is useful when only a portion of the volume of interest is to be simulated. Multiple mask files must be supplied per each variable if necessary.

Search neighbourhood parameters

Search neighbourhood represents a 3D ellipsoid describing anisotropy. It is defined in terms of:

- Angles of anisotropy direction (azimuth, dip and plunge), according to GSLIB convention;
- search radii in each direction expressed in the number of grid nodes;
- anisotropy ratios in each direction expressed as number of nodes representing a geological distance of 1. The ratios are used only for computing the distance from each node in the search neighbourhood to the central node;
- power of computing weight according to distance of each node found in the search neighbourhood.

The nodes inside the search neighbourhood are sorted according to their distance to the central node, from the closest one to the furthest one.

Homothety

In mathematics, a homothety is a transformation of space which dilates distances with respect to a fixed point (http://wiki.artofproblemsolving.com). This parameter allows relative scaling of the elements found in the training image when transferred to the simulation grid.

The input can be either in a form of fixed values for each anisotropy direction or provided in an image grid file over the extent of the simulation grid. Upper and lower bounds of the homothety values can be imposed for each anisotropy direction, either as fixed parameters or in a form of a grid image object.

Rotation

This parameter is useful when the spatial arrangement of the elements in the simulation grid is rotated in relation to the elements present in the training image.

Similar to the homothety, the rotation input can be in a form of fixed parameters for each angle (azimuth, dip, plunge) or as an input grid image file representing a potential field of azimuth, dip and plunge. Tolerance can be supplied in the two formats also.

This functionality can be useful when simulating mineralised elements within stratigraphically conformable units and the conditioning data for the bedding is available in a form of structural measurements of the drill core. In this case, it is possible to create a potential field of the bedding and derive three separate input files – for the azimuth, dip and plunge components.

Consistency of conditioning data

This parameter, used in simulation of continuous variables, represents the maximum accepted expansion in both extremities of the range of values in the training image for covering

the conditioning data values. For example, if this number is set to 0.1, the conditioning data values can be beyond the range of the values in the training images (in both extremities) to at most 10%.

Maximal number of neighbouring nodes for each variable

The parameter describes the conditioning dataset – the maximum number of nodes n in the simulation grid closest to the node x being simulated, which are to be used within the search neighbourhood for each variable.

Distance threshold

The parameter defines the allowed variation in the distance being searched for in the training image. It needs to be specified because a TI pattern matching a data event d_n exactly is often not found. When the distance between the TI pattern and d_n is smaller than t, the central node of the TI pattern is pasted at location x. The distance is measured on the fraction of non-matching nodes for categorical simulations. All distances are normalized ensuring their minimum to be zero (exact match) and their maximum to be 1 (no match). The parameter needs to be provided for each variable to be simulated.

Probability constraints

Probability constraints can add extra conditioning to the categorical variable simulations. Global or local probability constraints can be used.

Maximum scan fraction for a training image

This parameter represents the volumetric fraction of the TI to be scanned when searching the TI for suitable matches to the data events. It limits the number of TI patterns that are scanned for their similarity with d_n. It ranges from 0 (no scan) to 1 (scan full TI if necessary). If the maximum fraction of the TI is scanned and still no TI pattern with acceptable distance is found, the central node of the TI pattern with the lowest distance is pasted at the location x.

2.2 Simulation of grade

A widely accepted form of simulation for continuous variables is Sequential Gaussian Simulation. The underlying algorithm of SGS is simple kriging. Kriging provides an estimate of both the mean of the variable of interest and its standard deviation at each grid node, meaning that the variable at each node is represented as a random variable following a Gaussian distribution.

The conditional distributions are inferred in the Gaussian space. As SGS requires univariate Gaussian distribution of the continuous variable, the variable must be transformed to standard

Gaussian space with the mean of 0 and the standard deviation of 1. The SGS algorithm then assumes multi-Gaussianity – conditional distribution of each of the co-located variables is assumed to be a random function of multivariate Gaussian form, where any linear combination of its variables follows a Gaussian distribution. The simulation takes place in this space. A variogram model based on the Gaussian units is used during the simulation. A random path is usually followed to avoid artefacts which are inevitable if the grid nodes are visited in a regular fashion. The simulation results are then backtransformed to the original units (Yunsel, 2012).

There are a few basic steps involved in the SGS workflow, they have been broadly covered in the literature:

1. Prepare input data for the SGS algorithm:
    a. Obtain a representative histogram for the input conditioning data;
    b. Transform the data into a Gaussian space;
    c. Produce a variogram model for the variable of interest in the Gaussian units;
2. Run the SGS algorithm, during which the following takes place:
    a. Generate a random path though the grid nodes;
    b. Visit the first node in the path and use kriging to estimate a mean and standard deviation at that node based on surrounding data. This is termed local conditional probability distribution function;
    c. Select at random a value from the local conditional probability distribution function and set the node value to that number;
    d. Include the newly simulated value as part of the conditioning data. All previously simulated values serve as part of conditioning data in order to preserve the proper covariance structure between simulated values;
    e. Repeat the steps 2a-d until all grid nodes have a simulated value.
3. Validate the results:
    a. Visual aspect of the simulated realisations;
    b. Statistics;
    c. Histograms;
    d. Variogram reproduction.

Adopting the multivariate Gaussian model for gold simulation is one of the simplest and most practical approaches to produce conditional representation of uncertainty for continuous variables (Deutsch, 2013).

3 PRACTICAL APPLICATION OF THE SIMULATION ALGORITHMS

The algorithms described in the previous chapter have been applied to a set of data originating from Nyankanga deposit, Geita gold mine. The dataset was chosen among other AngloGold deposits due to the fact that the local geology was expected to lend itself quite well to the MPS simulation. Also, extensive areas of the deposit have been drilled at dense spacing by grade control drilling, with lithological description of the chips available providing a good data set for a training image.

3.1 Geological settings

The Geita gold mine is located to the south of Lake Victoria in the northwest of Tanzania. It is hosted within the Sukumaland Greenstone Belt of the Lake Victoria goldfields. The Geita terrain is made up of greenschist facies rocks consisting of clastic sedimentary rocks, black shales, banded iron formation (BIF) and felsic volcanoclastics, which are intruded by a sequence of mafic to felsic rocks.

The geology of the Nyankanga deposit comprises lense-shaped BIF packages with intercalation of intermediate and felsic intrusives, termed “diorites” for brevity in the current report, and minor sedimentary rocks. The package is folded, faulted and sheared. Subsequently to deformation it has undergone hydrothermal alteration. The sequence is regularly cut by late-stage barren quartz-porphyry dykes. Along the strike of the orebody, the dykes converge and link, compartmentalising the orebody (Brayshaw, 2010).

Gold mineralisation is predominantly shear-controlled and closely associated with banded-iron formations. It is localised along a distinct, tabular, shallowly dipping shear zone. The intricacies of a braided fault zone controlling the mineralisation have local variability of a few meters. The highest grades are associated with breccia zones within BIF which are sigmoidal or tabular in shape (Nyankanga Resource Model Handover Note, 2013). Within the diorite, mineralisation is wider, but has a more erratic gold distribution and a lower average grade.

3.2 Data description

The simulation was undertaken in the Eastern part of the Nyankanga orebody to test the applicability of the workflow on a small portion of the deposit.

The location of the simulation volume in relation to the operating pit is shown in Figure 3.1.

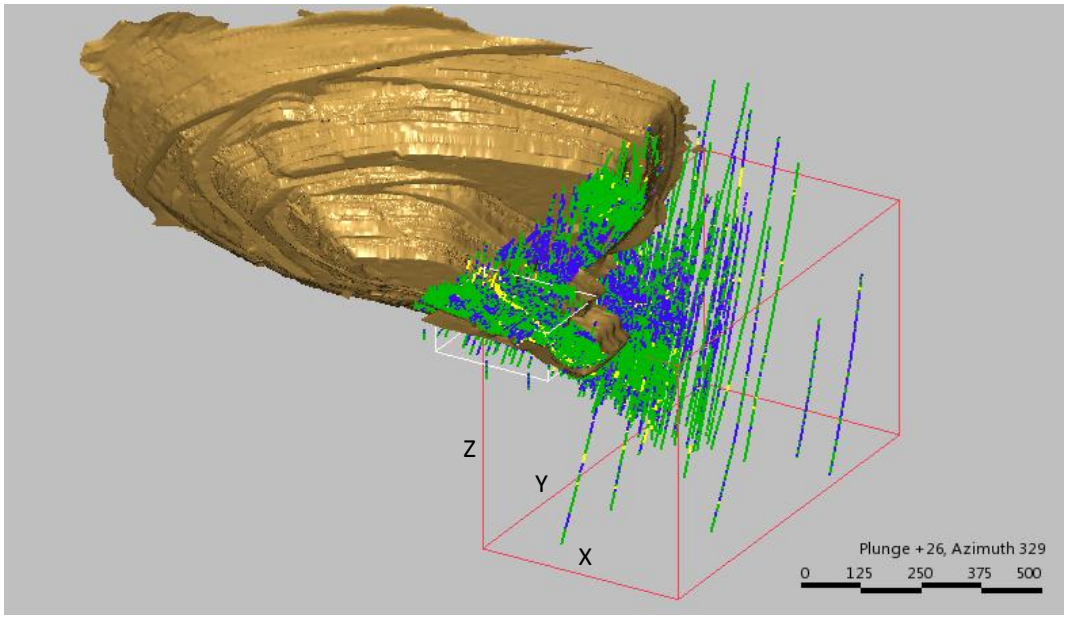

Figure 3.1. Isoclinal view of the Nyankanga pit showing drillholes dataset used in the simulation.
The white box represents the extent of the training image, the red box – main simulation volume.

The drillhole dataset comprised of 410 drillholes: 249 by reverse circulation (RC) and 161 by diamond core (DC) drilling. The majority of the drillholes are sampled at 1m intervals. In the top portion of the deposit, dense grade control drilling on a grid of 10m (along Easting) by 5m (along Northing) allowed to define a well-informed training image.

3.3 Conventions used in the report

Further in the report, where not specified explicitly, the following conventions are used:

- References to geographic directions are made in a modified metric coordinate system. Distance scales on figures are in meters;
- Gold values where reported have been modified. Unless otherwise specified, the same colour scale convention for gold was used for all the images in the report in order to allow comparison of the outputs of different processes. The gold statistics as well as appropriate units on graphs have been modified or excluded.

Colour coding schemes for lithologies, grade and measures of a unit, like probabilities, are presented in Figure 3.2.

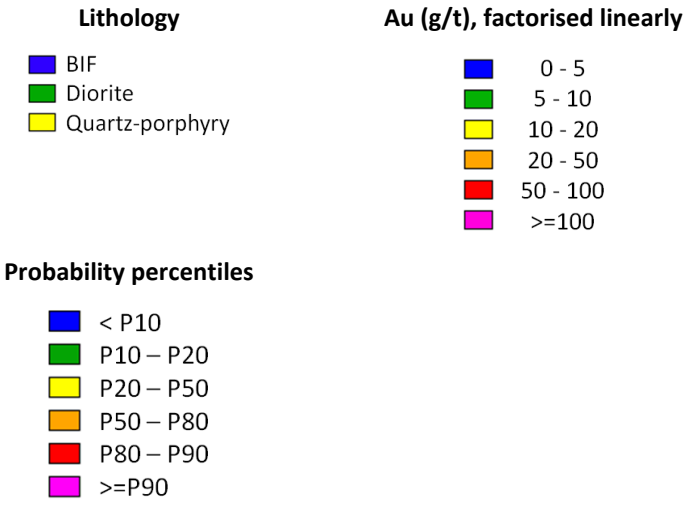

Figure 3.2. Legends used in the graphics of the report

3.4 Training image

Choice of a training image for simulation of lithologies is of paramount importance in the application of MPS. The training image serves as the source of spatial patterns to be simulated.

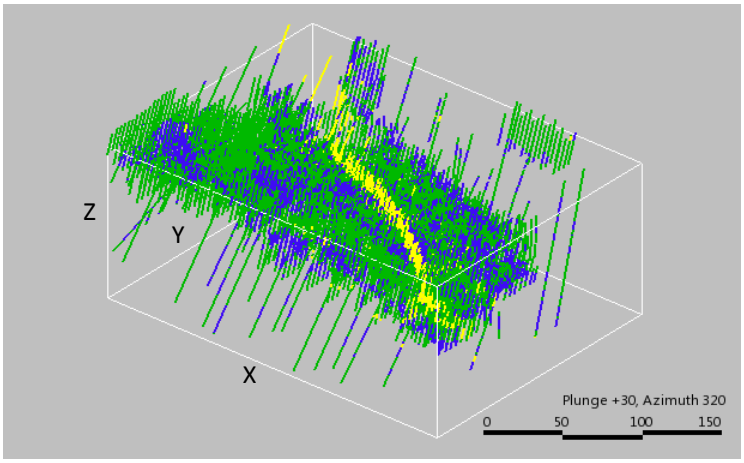

Figure 3.3. Drillholes used in the creation of a training image.
Interval colours display the logged lithology.

The training image with the total number of 742,500 nodes was created. Its geometry is presented in Table 3.1.

Table 3.1. Training image geometry

Parameter	X	Y	Z
Origin, m	50,426	10,050	1,071
Node spacing, m	2	2	2
Number of nodes	135	100	55

Densely spaced data allowed deterministic interpretation of the lithologies. The training image was defined only in a well-informed portion of the grid, the rest of the grid nodes were assigned undefined values.

Three main lithologies were modelled and used later as stationary domains for simulating gold values: banded iron formation, intrusive diorite complex, and barren quartz porphyry dykes.

Leapfrog software was used to create a geological wireframe model of the three main lithologies. The boundary between BIF and diorite was modelled using Radial Basis Function (RBF) method. Deterministic vein-type modelling approach was employed for creating tabular wireframes representing late barren dykes. The resulting wireframes were used to code grid nodes of the training image.

a) 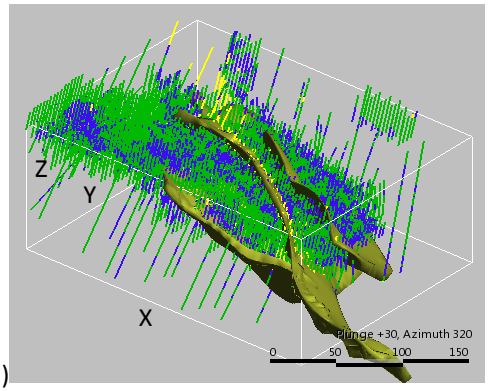

b) 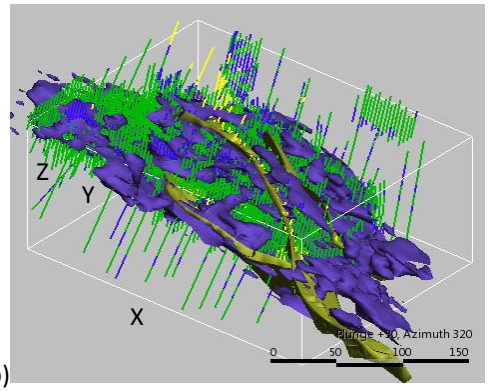

Figure 3.4. Wireframe model used to create a training image.
a) dykes, b) dykes and BIF.

A sectional view of the resulting training image is shown in Figure 3.5.

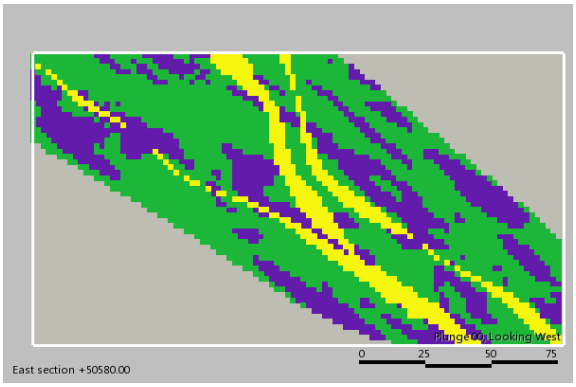

Figure 3.5. The three main lithologies in the training image.

The simulation algorithm was first tested on the training image, and only upon validation of the results it was implemented to the main simulation grid.

3.4.1 TI statistics

For the purpose of simulation, the statistics of the raw data must be representative. This involves eliminating bias. To ensure this, both the RC and DC drillhole samples were composited to 1m support and subsequently declustered.

Different cell sizes were tested. Based on the minimised average mean, the cell size of 30mE x 30mN x 10mElev for declustering was chosen.

The histograms of the declustered dataset in the training image are presented in Figure 3.6.

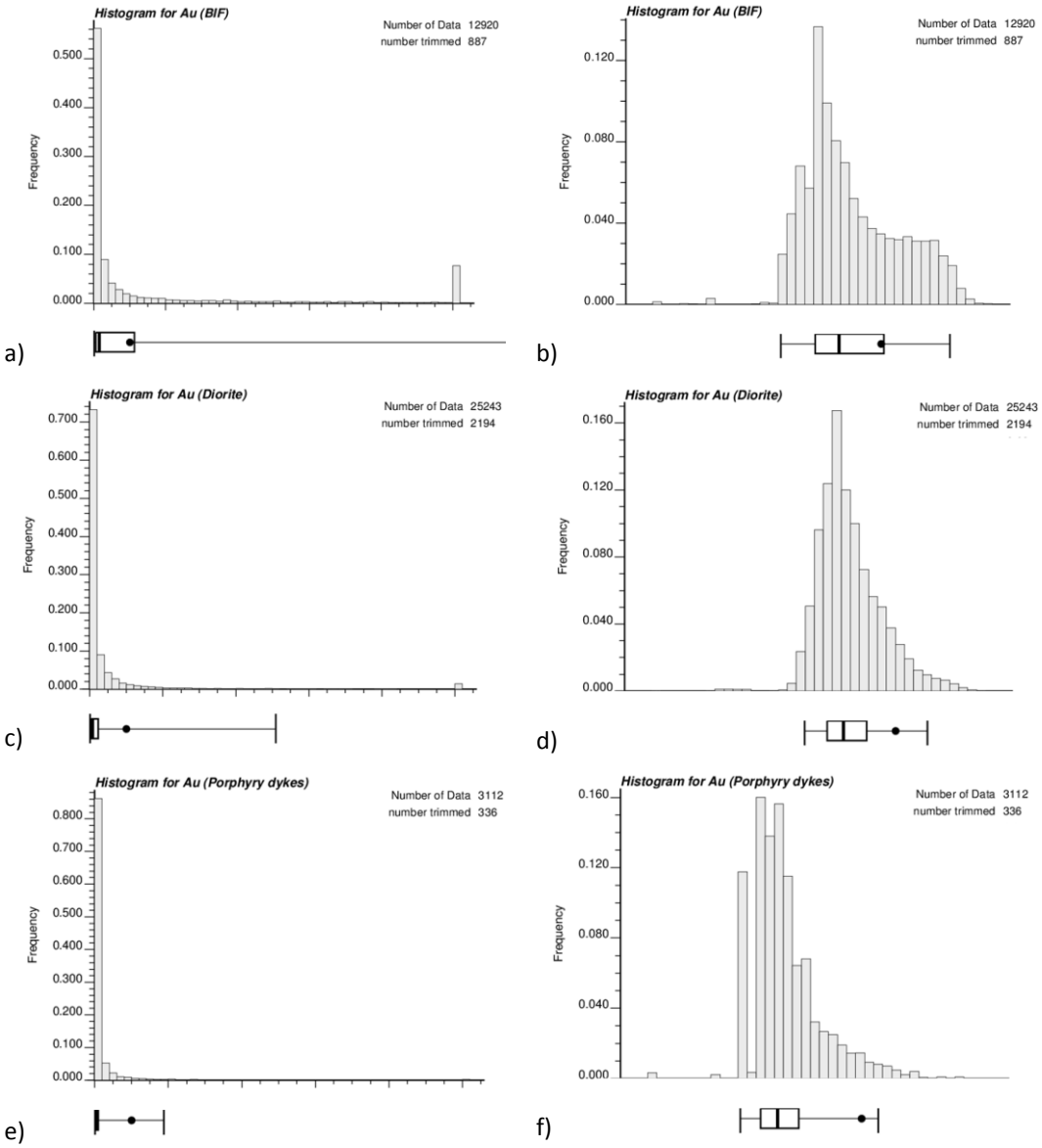

Figure 3.6. Au statistics of the conditioning data in the training image for the main lithology types. a), c) and e) histograms in the original units, b), d), and f) histograms in the log scale.

Gold in each of the three lithological units displays strongly positively skewed lognormal distribution. The mean value in each lithology is much higher than the median value. The interquartile range, a measure of spread around the median, broadens from quartz porphyry to that in diorite and in BIF.

The coefficient of variation is quite high in each lithology. The quartz porphyry dykes, even though are post-mineralisation and considered unmineralised, also have a few extreme values.

Despiking, necessary for smooth transform to Gaussian space, was done for each rock type. Despiking is performed to break ties when identical values are present in the dataset, e.g. default values assigned to the samples below detection limit. Further to this, the data was capped to eliminate outliers.

The dataset was normal-score transformed per lithology code for variogram modelling to be further used in grade simulation.

3.4.2 TI variography

Variogram modelling is required for two purposes: as input parameters for the SGS algorithm and to allow parametric validation of the simulation results.

The analysis of spatial correlation showed a greater spatial continuity in the NW-SE direction plunging towards NW. The azimuth of the primary anisotropy direction is shown in Figure 3.7.

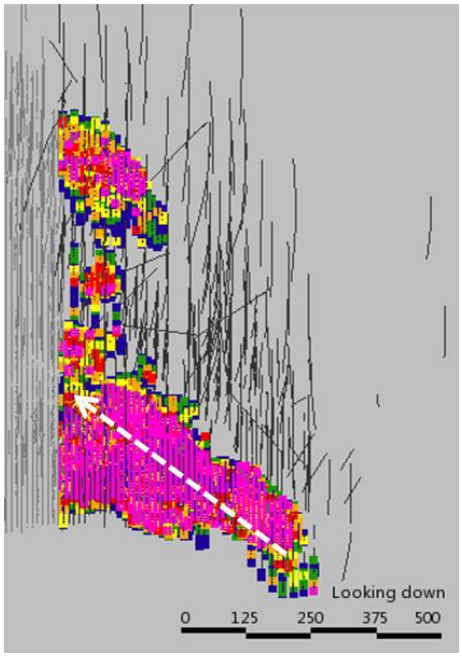

Figure 3.7. Plan view of the study area showing the primary direction of continuity.

The anisotropy was modelled along the same directions for the lithologies and grade. The anisotropy directions are summarised in Table 3.2.

Table 3.2. Anisotropy directions

Lithology	Anisotropy angles (Z/ X/ Y)	Angle component in Direction I	Angle component in Direction 2	Angle component in Direction 3
BIF/diorite	-55/ -20/ 40	-55.0 -20.0	-129.0 37.2	12.8 46.0
Quartz porphyry	-60/ -10/ 45	-60.0 -10.0	-140.1 44.1	20.1 44.1

The variogram model parameters for the interface between BIF and diorite are presented in Table 3.3. It was deemed not necessary to create an indicator variogram model for the dykes, the main validation tool for checking the continuity of dykes used further in the workflow was visual.

Table 3.3. Variogram model parameters for BIF/diorite interface

Lithology	Nugget	Structure ID	Structure Sill	Range in Direction 1	Range in Direction 2	Range in Direction 3
BIF/diorite	0.0	1	0.40	8.0	8.0	2.0
		2	0.35	15.0	15.0	9.0
		3	0.25	50.0	50.0	11.0

The variograms for gold values were produced both in original and in Gaussian space and are summarised in the Tables 3.4 and 3.5.

Table 3.4. Variogram model parameters for gold in original space

Au domain	Nugget	Structure ID	Structure Sill	Range in Direction 1	Range in Direction 2	Range in Direction 3
BIF	0.14	1	0.34	8.0	55.0	3.0
		2	0.52	47.0	38.0	12.0
Diorite	0.20	1	0.50	22.0	25.0	11.0
		2	0.30	32.0	32.0	11.0
Quartz Porphyries	0.15	1	0.30	4.0	17.0	5.0
		2	0.30	22.0	30.0	6.0
		3	0.25	90.0	30.0	7.0

Table 3.5. Variogram model parameters for gold in Gaussian space

Au domain	Nugget	Structure ID	Structure Sill	Range in Direction 1	Range in Direction 2	Range in Direction 3
BIF	0.10	1	0.25	4.0	5.0	4.0
		2	0.28	52.0	65.0	18.0
		3	0.37	125.0	70.0	20.0
Diorite	0.10	1	0.45	10.0	9.0	5.0
		2	0.35	47.0	45.0	19.0
		3	0.10	100.0	70.0	19.0
Quartz Porphyries	0.10	1	0.30	10.0	3.0	5.0
		2	0.30	22.0	8.0	12.0
		3	0.30	50.0	45.0	12.0

Comparison of the variogram models produced for gold in original units versus the models in Gaussian space shows longer ranges in Gaussian space. It is specifically true for BIF and to a less

extent for diorite. For the latter, 90% variance is reached at 45m for the first and second directions of continuity. It is 30% longer that the ranges in the original units. A complete set of the variogram models can be found in Appendix A.

The variogram models in Gaussian space, based on the densely spaced grade control sampling, were used for further simulation of gold in the main simulation volume.

3.4.3 Validating a training image

A test for reasonableness of the parameters was done by first performing a full simulation exercise on the training image volume.

Sensitivity of the Direct Sampling algorithm to different parameters was tested to balance the simulation quality and processing time. The test was done by fixing all the parameters and modifying one parameter at a time. Recommendations provided in Mariethoz et al (2012, 2013) were followed to allow reasonable results in minimal time.

The following DS parameters were deemed sufficient for the good reproduction of the lithologies:

- Node spacing. The node spacing is a critical factor in the process. As a first run, a grid of irregular spaced nodes was used (5mE x 5mN x 2mElev). This spacing was chosen to resemble the drillhole sample spacing of 10mE x 5mN x 1mElev. Visual inspection of the simulation results was difficult for the non-cubic grid cells. For the final training image the grid was modified to have nodes of cubic geometry spaced at 2m in each direction;
- Consistency of conditioning data: 0.05;
- Anisotropy radii: 10-10-5 for the primary, secondary and tertiary directions of anisotropy respectively;
- Anisotropy ratio: 1-1-1;
- Number of nodes n=30, although n=24 produced sufficiently good results also;
- Distance threshold: 0.05;
- Maximum fraction of the training image to be scanned: 0.3.

The processing time with the above settings was 9 min per lithology realisation, for a grid size of 742,500 nodes and a conditioning dataset of 45,700 points. One realisation of SGS took approximately 0.5 min per lithology type.

A simulation for 50 realisations was done for both lithology and grade within the training image volume. The gold realisations were “stitched” to those of lithology in a sequential order.

The results of the trial simulation were checked for visual reproduction, global proportions, histograms and variograms reproduction.

Visual inspection

Prior to using the training image for the main volume simulation, unconditional simulation was performed to ensure good overall reproducibility of the patterns found in the training image and to confirm the choice of simulation parameters. A comparison of the training image and the unconditional simulation patterns is given in Figure 3.8.

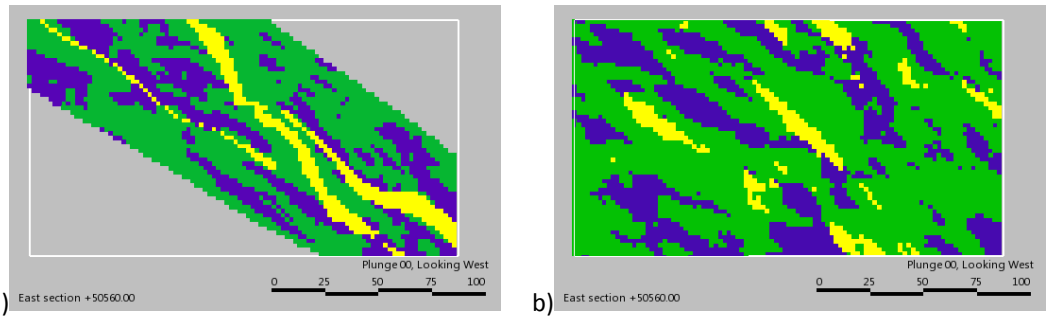

Figure 3.8. Unconditional simulation of lithology, sectional view.
a) training image with the three main lithologies, b) one unconditional realisation within the training image volume.

In the unconditional simulation, the connectivity of dykes posed a major challenge while simulated BIF and diorite shapes were reproduced quite reasonably and displayed the same level of irregularity of the shapes as in the training image. A number of parameters were tested, but none of them seem to have improved the connectivity dramatically.

A better connectivity of dykes was achieved when running a conditional simulation within the training image volume. A big factor was the high density of the conditioning data. Examples of the conditional simulation are displayed in Figure 3.9.

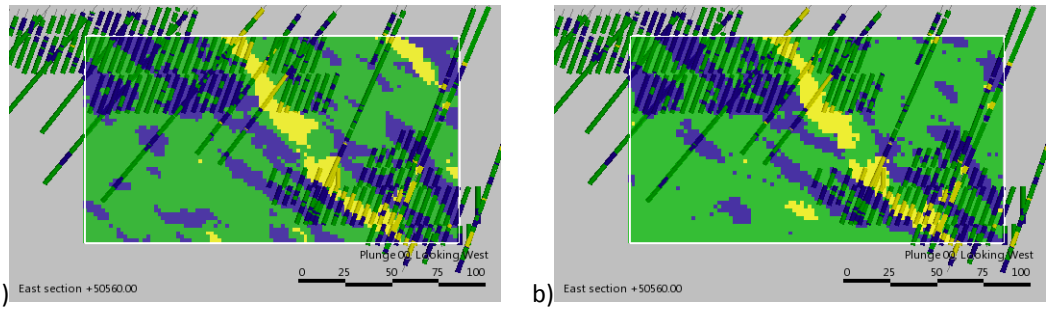

Figure 3.9. Conditional simulation within the volume of the training image, sectional view of two realisations.

The honouring of the global lithology proportions within the training image conditional simulation was good taking into consideration the fact that no global proportions were specified in the simulation input. The BIF was understated and the diorite overstated in the simulation by 4-5%. The comparison is presented in Table 3.6.

Table 3.6. Global proportions of the conditionally simulated lithologies within the training image

Lithology	Conditioning data	Simulated proportions
BIF	0.31	0.27
Diorite	0.61	0.66
QP	0.08	0.07

Statistics and histogram validation

The results of the gold simulation were tested by comparing the main statistics of the gold distribution, and visually for honouring of the conditioning data. Histograms for all three lithology types were very close to those of the conditioning data, they are presented in Figure 3.10.

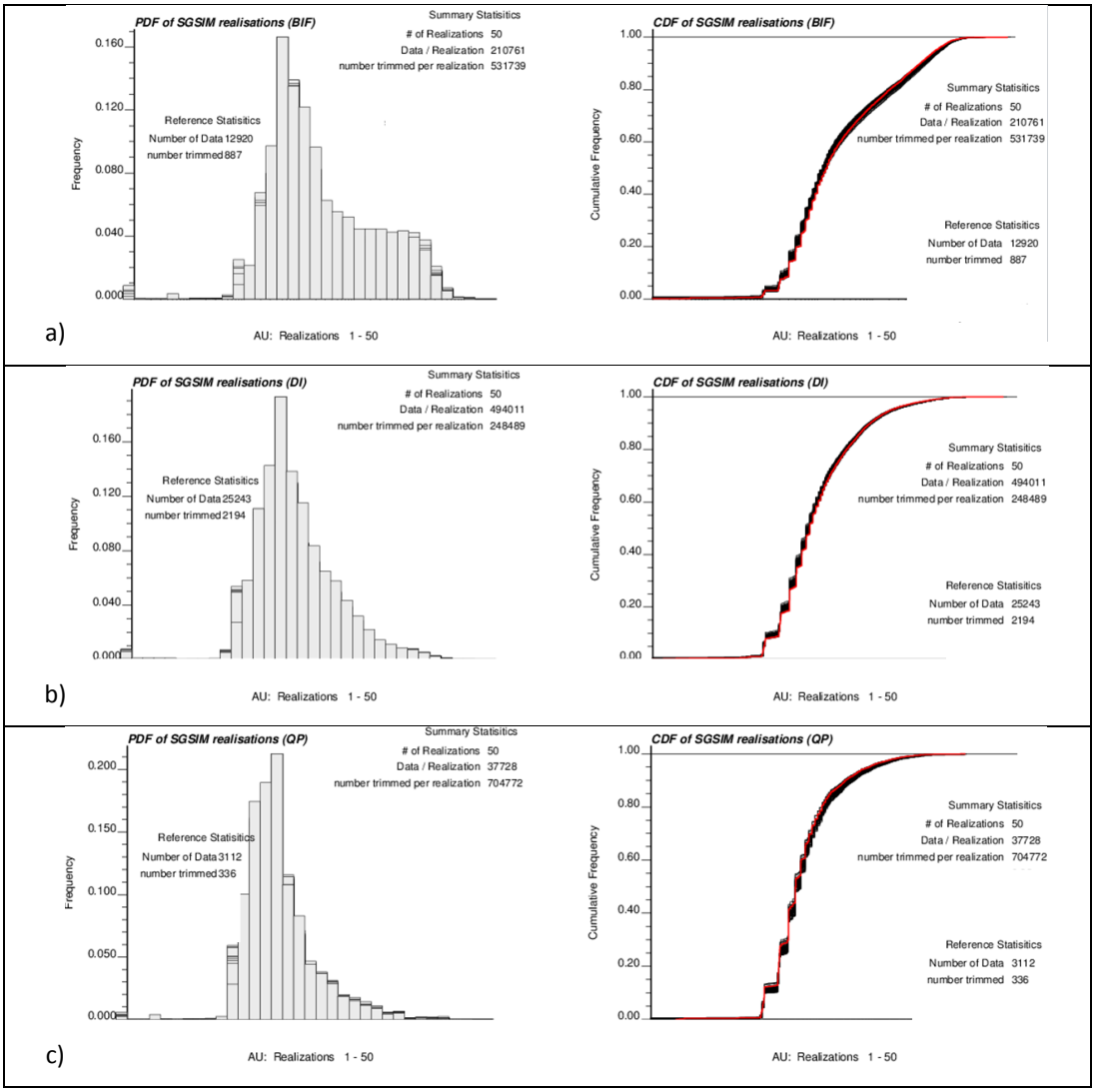

Figure 3.10. Histogram reproduction within the training image.
pdf and cdf graphs of a) BIF, b) diorite, c) quartz porphyry.

Variogram validation

Variograms of the realisations were compared to the indicator variograms for lithologies and gold within each of the rock types, in the principal directions of continuity. The comparison was done within a portion of the simulated volume for brevity. The results display very good reproduction of the continuity for both lithologies and grade within them. The lithology variograms are presented in Figure 3.11.

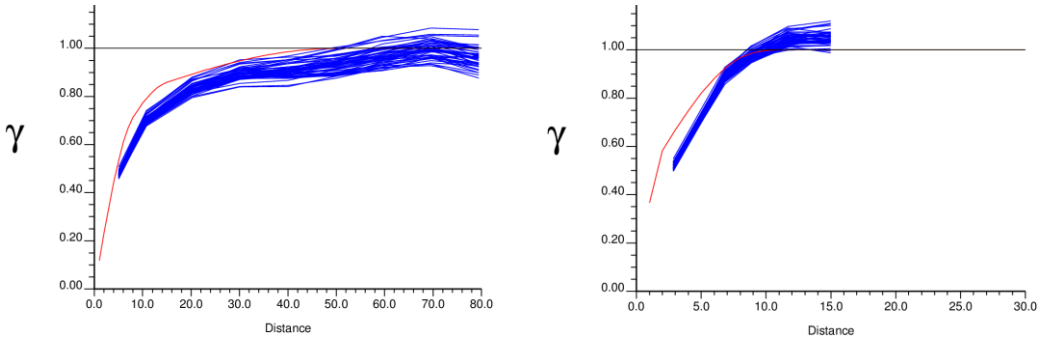

Figure 3.11. Variogram reproduction for the simulated lithologies (BIF and diorite).
a) Primary and secondary directions of anisotropy compared to an input omni-directional variogram, b) comparison for the third direction of anisotropy.

Variograms of the simulated gold values were validated for each of the three main lithologies. The comparison was done against the variogram model created in the original space. For brevity, the simulated variograms were summarised in the easting, northing and elevation directions, not in the principal directions of the continuity, hence the comparison is not direct. Overall, the ranges of continuity are well replicated in the simulation. The gold variograms can be found in Appendix B.

3.5 Simulation of the main area

The main simulation for a more extensive volume was done for 50 realisations of both lithology and gold.

The best traditional approach in simulation is to generate 100-200 realisations (Deutsch, 2013) to stabilise the uncertainty and reduce "uncertainty of the uncertainty" as much as possible. There are too many subjective decisions that might aggravate the uncertainty if a small number of realisations is produced.

The simulation grid consisting of 1,827,360 nodes covered the extent of 470mE by 900mN by 540mElev. The geometry of the simulation grid is presented below:

Table 3.7. Geometry of the main simulation grid

Parameter	**X**	**Y**	**Z**
Origin, m	50422.5	10252.5	532.5
Node spacing, m	5	5	5
Number of nodes	94	180	108

Prior to deciding on the node resolution, a consideration was given to the size of the selective mining units (SMU) and the size of the panels. The size of the SMU used for Nyankanga is 10mE by 10mN by 3.33mElev. The size of the panels is 40mE x 40mN x 10mElev. The vertical dimension of the SMU is awkward to work with for upscaling of realisations at a later stage. It was decided to work with cubic grid cell of 5m side dimension to accommodate smooth upscaling to the panel size at a later stage. A resolution coarser than that in the training image was chosen also for time efficiency reasons. For the same reason, a mask object was used to block out the simulation grid nodes away from the mineralised shear zone.

The DS simulation parameters that produced good results in the simulation runs over the training image volume were used in the large scale simulation, and fine-tuned further.

3.5.1 Lithology simulation

50 realisations of lithology were performed. An extensive validation was done similar to the routine described above for the training image volume simulation.

Visual validation

Reproduction of the patterns found in the training image was very good for diorite and BIF categories. The issue of poor connectivity of the dykes re-immerged. Running a number of sensitivity studies while modifying one parameter at a time allowed comparison of the different runs to test the effect on the connectivity.

Adding global proportions conditioning had a slightly deteriorating effect on the continuity as demonstrated in Figure 3.12.

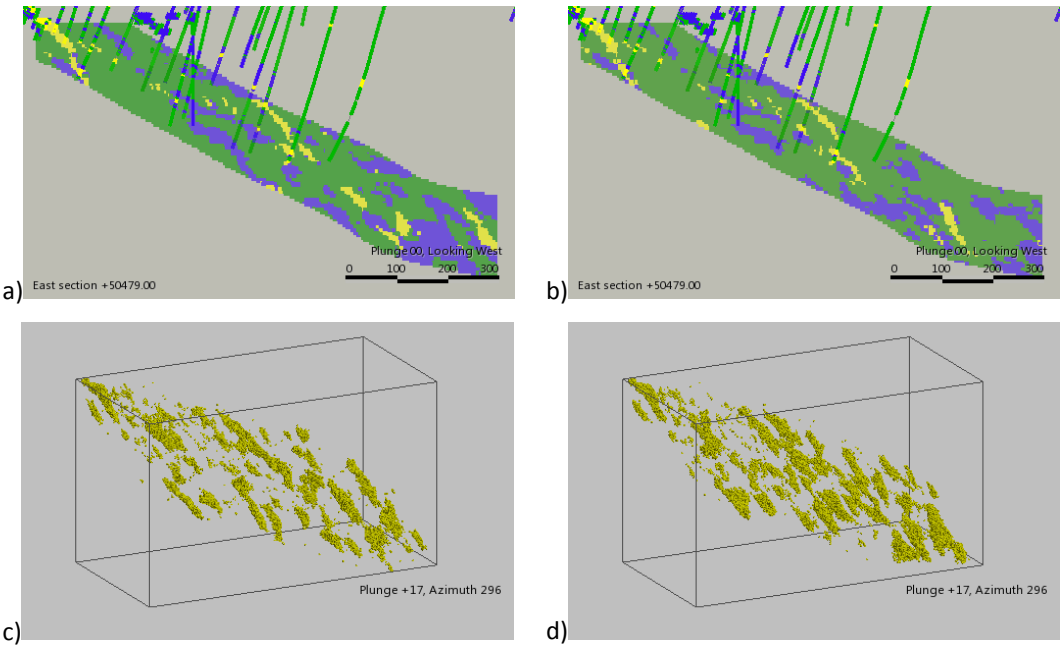

Figure 3.12. Conditional simulation of lithology over main grid, sectional and isoclinal views.
a) and c) simulation with global proportions conditioning, b) and d) simulation without global proportions.

To enforce better dyke continuity, at least in the vicinity of the drillholes, a conditioning grid object was used in the input for the simulation in addition to the drillhole samples. The grid object was created for the same volume as the simulation grid, with nodes flagged in the vicinity of the drillhole intervals that intersected dykes. The flagging was achieved by coding the grid nodes falling within a distance of 20m from the appropriate drillhole intersections, using Leapfrog software. The continuity within the conditioning dykes was improved. This approach had an outcome similar to that with locally varying proportions. Figure 3.13 demonstrates this – the upper part of the simulation grid has higher content of nodes simulated as dykes than the portions down the plunge. This is explained by the higher density of drill coverage in the upper portions of the volume.

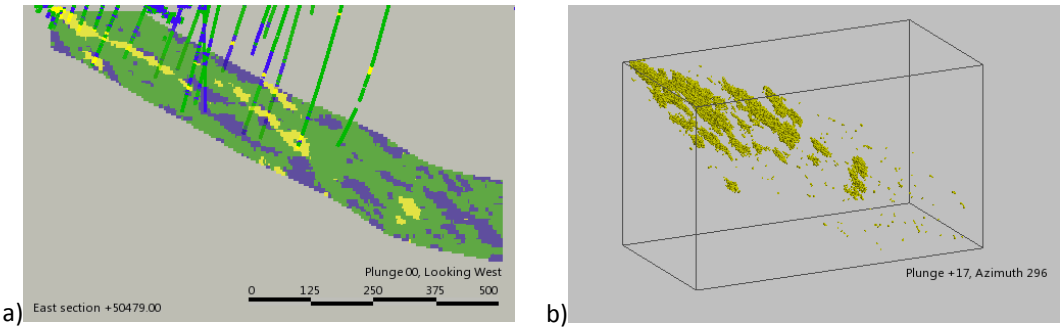

Figure 3.13. Conditional simulation of lithology over main grid, dykes conditioned by an additional grid object.
a) sectional view, b) isoclinal view.

Further to the above, other parameters were tested to improve the continuity of the dykes, such as increasing number of nodes, increasing distance threshold tolerance, increasing search neighbourhood radii. None of it resulted in any significant improvement while imposing higher computational demands.

A second training image was created and used as an additional input to the DS simulation. Equal weights of 0.5 were assigned to the two input training images. The extent of the new training image covered the whole volume of the simulation grid. It had a deterministic interpretation of the dykes produced from a wireframe model. No large scale interpretation of the BIF/diorite interface was available at the same scale. To substitute for this, dummy values were assigned to the nodes in the training image representing the host rock to the dykes as follows: the training image volume was split in three portions: upper portion was assigned codes of 1 (BIF), lower portion was assigned values of 2 (diorite), and an undefined zone was left in the middle between the two.

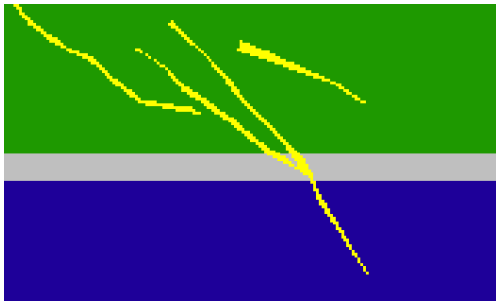

Figure 3.14. Second training image over the extent of the simulation volume, containing large-scale morphology of the dykes, sectional view.

The resulting simulation produced much better dyke connectivity as can be seen in Figure 3.15, however the BIF/diorite interface was not representative. Testing for the connectivity was terminated at this point to possibly be carried out in future.

a) 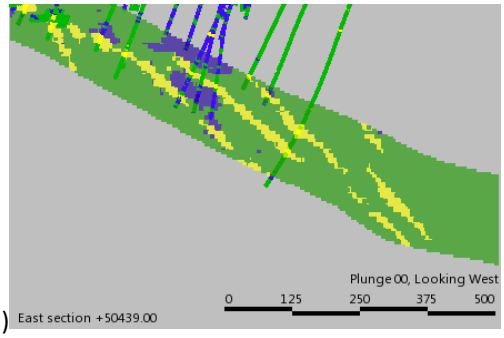

b) 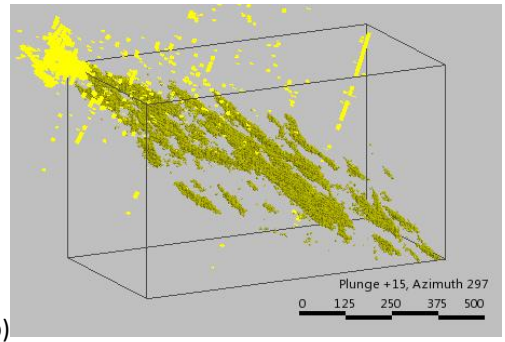

Figure 3.15. Lithology simulation using 2 training images.
a) sectional view, b) isoclinal view, the drillhole intervals logged for quartz porphyry dykes are displayed as yellow segments.

Analysis of the drillhole intersections through dykes in 3D showed that they have a radial attitude joining down dip with a plug-like intrusive body present in the top right corner of the

simulation grid. This can be seen in Figure 3.16. For future simulation work, it is suggested that a synthetic training image is used with a horizontal attitude of dykes and a rotation field defined over the whole volume of the simulation grid. This potential field can be created from the structural readings of the diamond core contacts. Simulation of the plug-like volume would require defining another stationary domain and yet another training image.

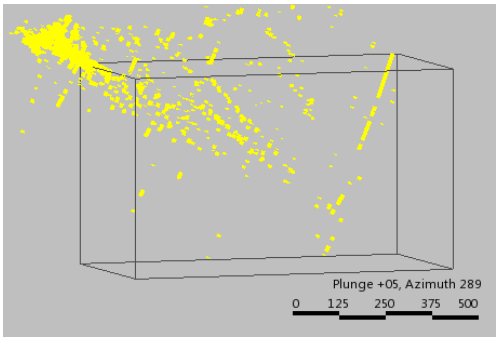

Figure 3.16. Dykes logging in the drillholes, isoclinal view.

Comparison of four realisations of lithology for the final simulation run demonstrates a uniqueness of each realisation, specifically further away from the conditioning data.

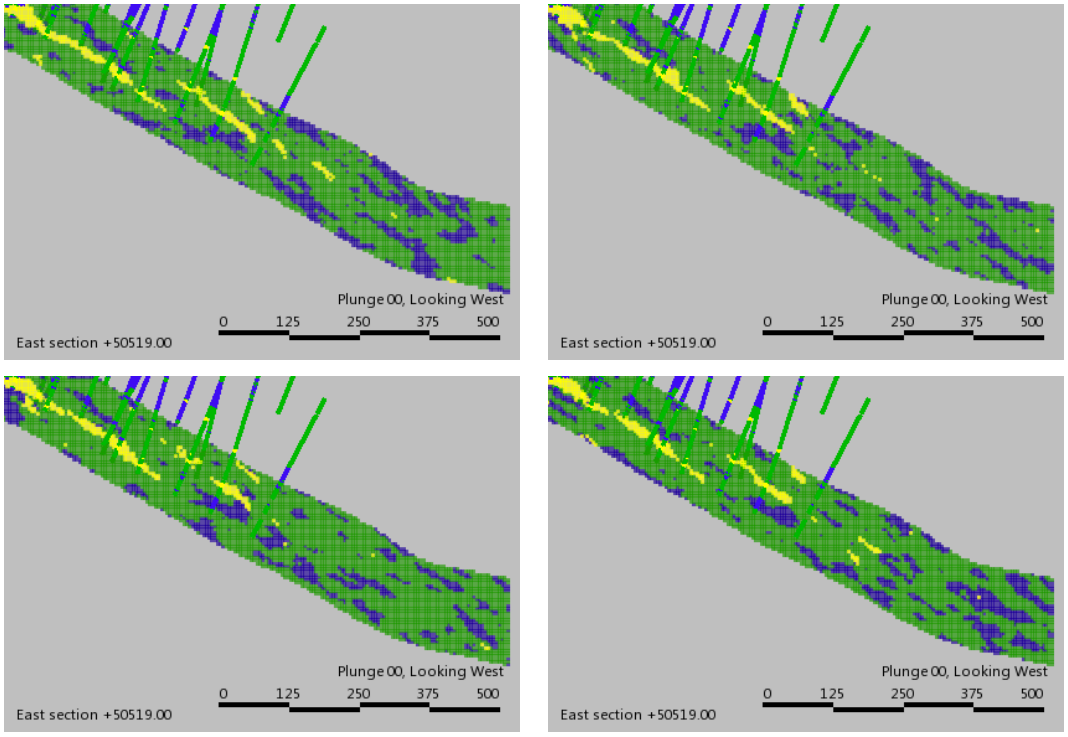

Figure 3.17. Four realisations of lithology from the final simulation run, sectional view.

For possible future simulation of the deposit, incorporation of structural readings for lineation will be useful for simulation of BIF/diorite interface. It will allow reproduction of geologically viable scenarios where diorites would have intruded along planes of weakness associated with bedding.

Global proportions

The global proportions used as an additional input for the simulation were determined from the logging information of the conditioning drillholes. Overall, the average values for the simulated global proportions are maintained. A few-percent overall fluctuation was observed across the 50 realisations and is shown in Table 3.8.

Table 3.8. Comparison of the simulated and input global lithology proportions

Lithology	Proportions in the conditioning drillholes	Proportions in the training image	Proportions in the 50 simulated realisations
BIF	0.29	0.28	0.26
Diorite	0.67	0.63	0.72
QP	0.04	0.09	0.02

The final proportions of the BIF are understated by 3%, in dykes the understating is by 2%, resulting in the overstatement of the presence of diorite by 5%.

The variation is attributed to insufficient understanding of the controlling parameters of the global proportions input for the Direct Sampling algorithm. Further work beyond the scope of the current project can be undertaken in this direction.

Figure 3.18 shows the histograms of the simulated proportions. The spread across the realisations is very narrow.

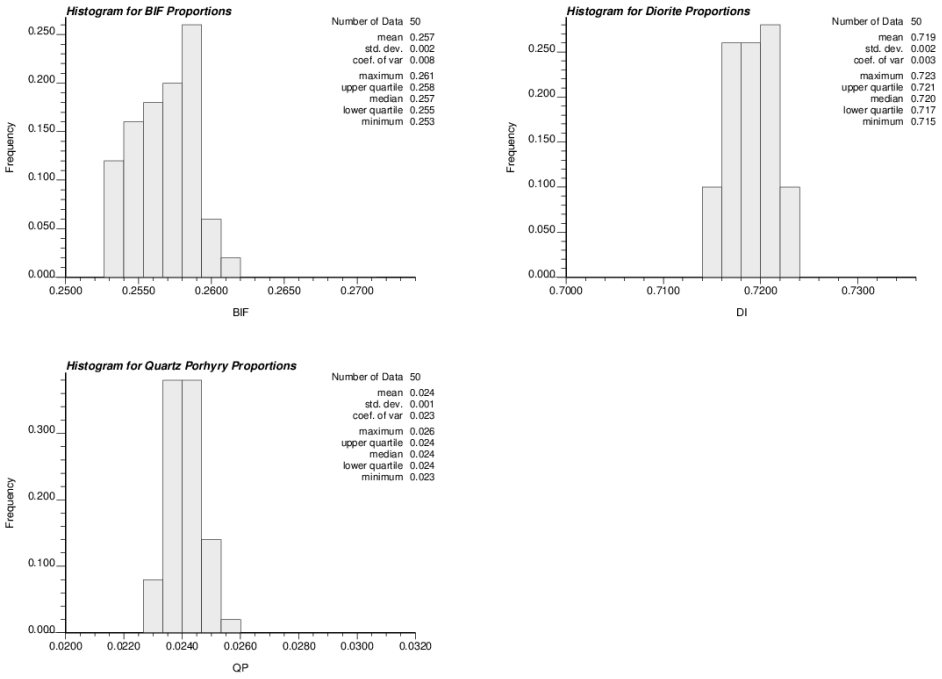

Figure 3.18. Histograms of the simulated lithology proportions across the 50 realisations.
a) proportions of BIF, b) proportions of diorite, c) proportions of quartz porphyry.

Despite the few percent deviations of the final proportions from the conditioning data it was decided to continue with the parameters for the simulation as the effect was considered to be immaterial.

Variogram reproduction

The variogram validation for the interface between the BIF and diorite was done for a representative portion of the simulation grid in the principal directions of continuity. The results are shown in Figure 3.19.

The simulation variograms between the BIF and diorite produced slightly longer ranges of continuity than the input model. A further investigation can be undertaken in future to understand the reason behind it.

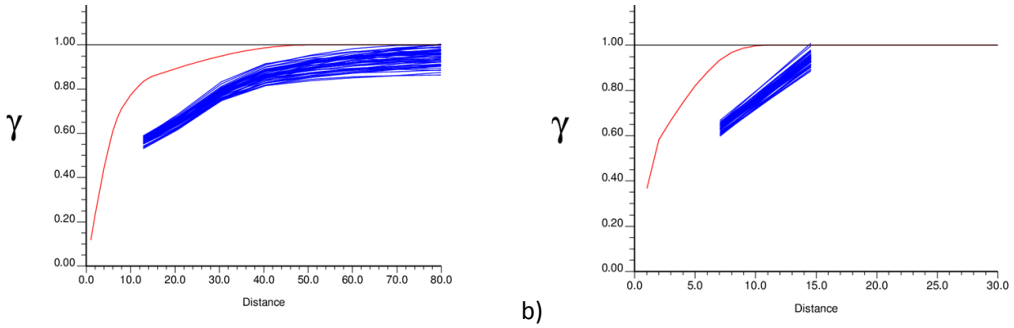

Figure 3.19. Variogram validation for the 50 lithology realisations.
a) Omnidirectional variograms in the plane of continuity, b) variograms in the third direction of continuity.

DS final simulation parameters

The algorithm was run in multi-thread mode. The only draw-back of using this mode of DS is that the exact reproduction of the simulation results is not guaranteed for the same random seed. The average time required to produce a single realisation for the main simulation grid was 21 minutes.

A number of parameters have been tested to balance the simulation quality and processing time. The following was found to produce acceptable results while not imposing high demands on the processing. These were used in the final simulation:

- Conditioning data:
  - drillhole samples (44,780);
  - a grid image containing quartz porphyry dykes' control points in the vicinity of the intersecting drillholes;
- Consistency of conditioning data: 0;
- Anisotropy radii: 10-10-5 for the primary, secondary and tertiary directions of anisotropy respectively;
- Anisotropy ratio: 1-1-1;

- Anisotropy angles: -55/-20/40;
- Number of nodes: 30;
- Distance threshold: 0.05;
- Distance tolerance for flagging nodes: 0.01;
- Probability constraints:
    - Global pdf proportions 0.29 (BIF), 0.67 (diorite), 0.04 (quartz porphyry);
    - Comparing pdf method: Kullback-Leibler divergence (KLD);
    - Probability deactivation distance: 4;
    - Constant threshold 0.002;
- Maximum fraction of training image to be scanned: 0.3.

The 50 realisations of lithology were used for subsequent geostatistical domaining of the simulated gold grade.

3.5.2 Grade simulation

An SGS simulation comprising 50 realisations of gold was performed.

Similar to any other estimation technique, data preparation for SGS must be thorough and requirements of representativeness, stationarity, and Gaussianity must be considered.

Prior to running Gaussian simulation, the conditioning drillhole samples were composited to the same support of 1m. The composite data was debiased and declustered to eliminate conditional bias due to possible oversampling of the high grade areas. Log probability plots and variance plots were analysed to facilitate the decision on grade capping. For each of the three lithologies the proportion of the capped samples to the total number of samples was below 1%. The mean of the gold values has dropped after capping with 6% for BIF, 11% for diorite and as much as 29% for porphyries.

The debiased data was further declustered per each lithological domain. Due to sparser drillhole spacing in the volume of the simulation grid in comparison to that over the training image volume, the results of the declustering test suggested to use a different declustering cell size. The final declustering was performed to the size of 100m in each direction, for each rock type.

Prior to performing the grade simulation, the data was despiked per lithology type.

The simulation was run for each lithology, the transformation of the gold values to the Gaussian space and back is built-in within the SGS algorithm. The set of Gaussian variogram models based on the densely spaced grade control drilling was supplied as an input to the simulation of grade in each lithology.

The simulated realisations of the gold grade were “stitched” to the previously simulated lithologies in sequential order. As such, the compiled file contained three gold values attributed

to each grid node of the simulation grid – one value per lithology type. The final Au grade was obtained by assigning to each node a gold value in accordance with the lithology simulated at the respective node.

The resulting gold grade simulations were validated per the same check list as for the training image, and included visual checking, validation of the statistics, and variogram checking.

Visual validation

The first four realisations of the grade are presented in Figure 3.20.

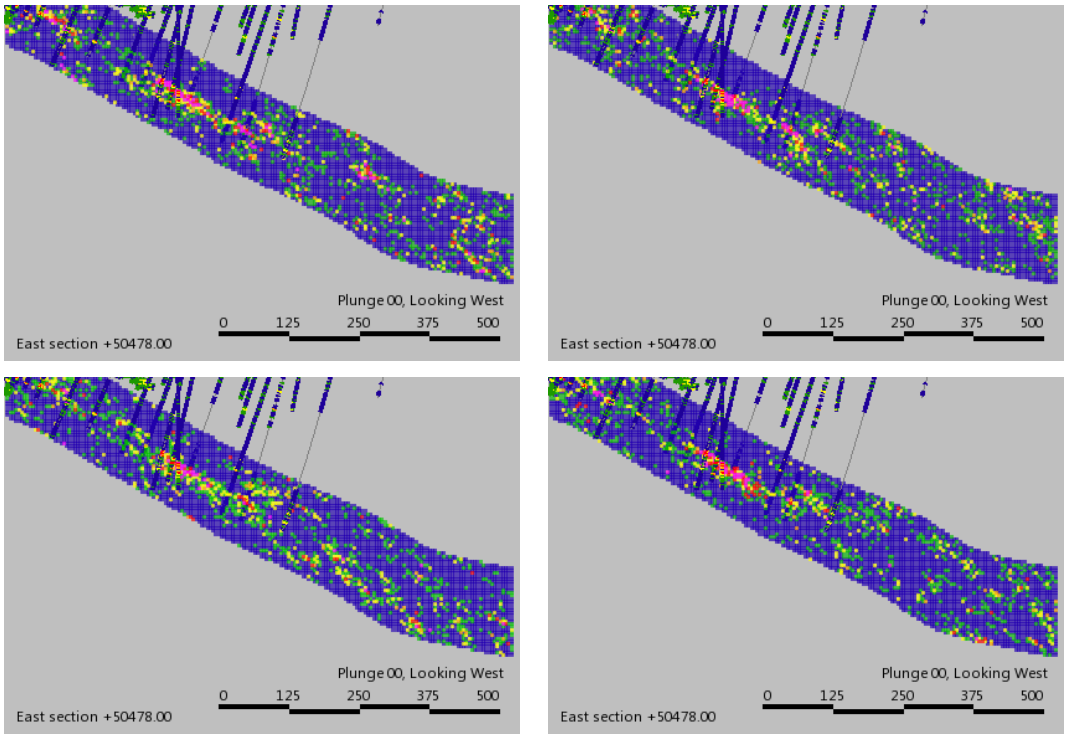

Figure 3.20. Four realisations of gold grade, sectional view.

While honouring of the drillhole samples is observed in each of the realisations, the appreciation of the uniqueness is apparent. The realisations display considerable variability away from conditioning data. The four realisations depict the short-range variability inherited from the variogram models of the densely spaced data in the training image. The differences between the realisations represent the joint uncertainty: from the lithology simulation and grade realisations within it.

Statistics and histogram reproduction

The histograms of the gold values for all realisations are plotted together with input histograms per lithology type and are shown in Figure 3.21. The reproduction of the histograms is good.

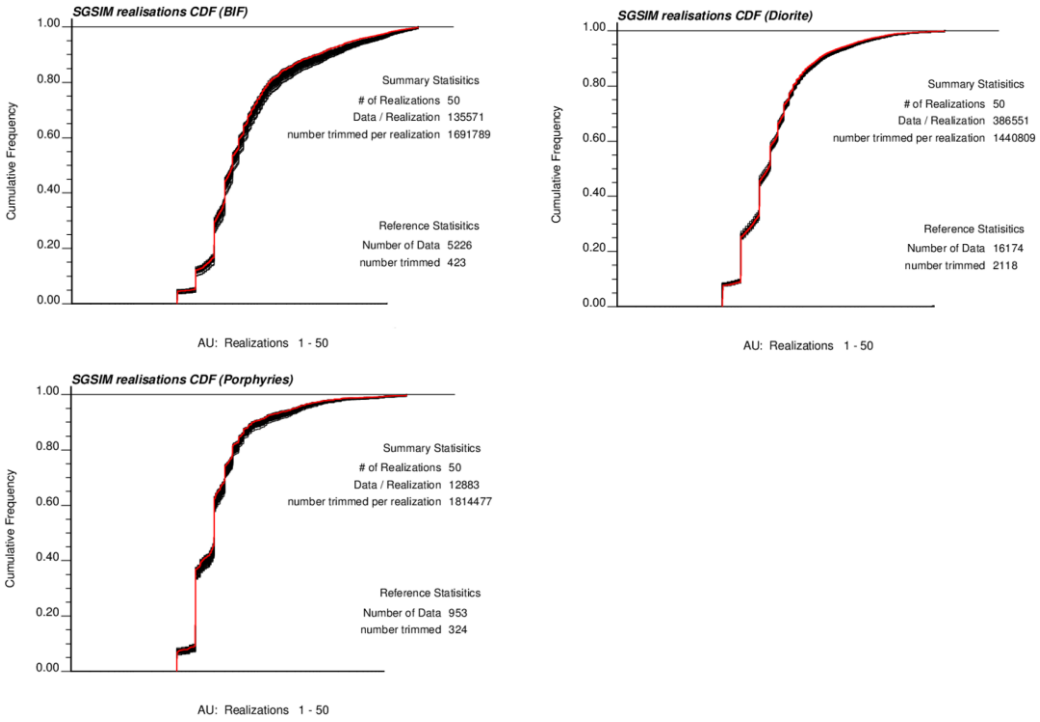

Figure 3.21. Histograms of the simulated gold values vs conditioning data.
a) BIF, b) diorite, c) quartz porphyry.

Variogram reproduction

Gold variogram reproduction was checked within a small portion of the simulation grid. The validation was performed for the three principle directions of anisotropy. The comparison was done against the variogram models based on densely spaced training image drillhole data, only for the BIF and diorite domains, since considerable care was taken to reproduce the connectivity of the barren dykes. The variograms for BIF and diorite domains are shown in Figure 3.22 and Figure 3.23. The comparison was done for the variograms constructed in the original data units.

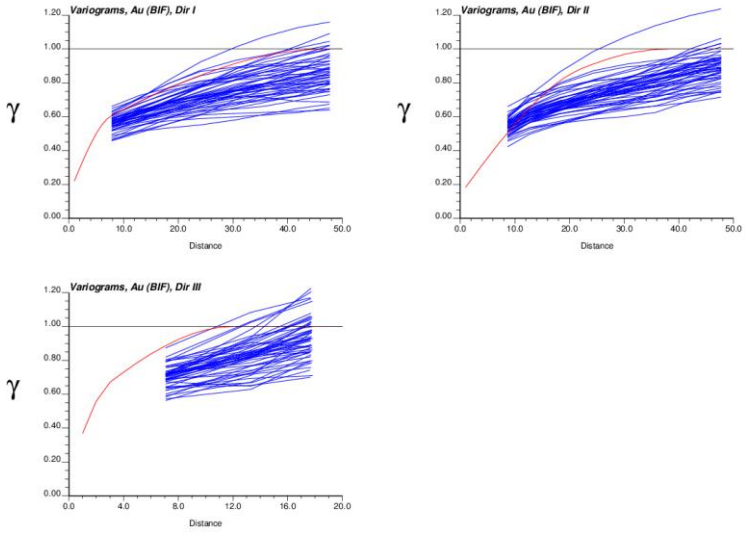

Figure 3.22. Variograms of the simulated gold realisations of BIF for the three principal directions of continuity.

While the gold variograms within the BIF domain display a good fit with the original model, the diorite variograms are not well behaved and show a high degree of variance against the original model, specifically in the second direction of continuity as seen in Figure 3.23.

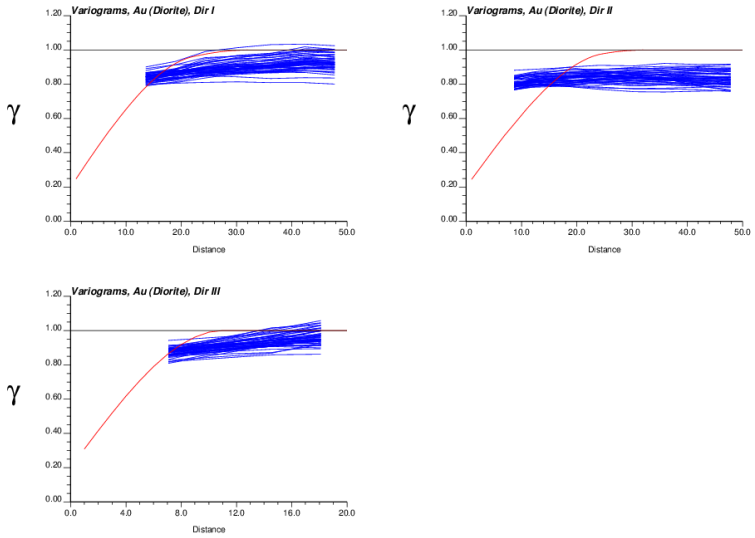

Figure 3.23. Variograms of the simulated gold realisations of diorite for the three principal directions of continuity.

The noise in the variograms of the diorite at a short scale distance is attributed to the fact that the model in the original space reaches 70% of variance within the range of 22-25m for the main continuity plane. This distance, expressed in terms of the simulation grid nodes, represents separation of 2-3 nodes as the orientation of anisotropy is oblique to the geometry of the simulation grid. Finer resolution simulation grid would be beneficial to allow reproduction of short scale continuity. Another explanation is that inadequate care has been taken in deciding on the extents of the volume for variogram validation. The volume spanned across the shear zone boundary and contained samples of high and low grade stationary domains, therefore noise was introduced into the variograms and the comparison with the high grade variograms of the training image was not valid.

3.6 Discussion

A number of techniques have been applied in a nested fashion during the lithological modelling. They vary through the spectrum of the techniques available for geological modelling. The best approach to geological modelling progresses from deterministic to more stochastic and is summarised as follows (Deutsch, 2013):

- Deterministic interpretation of geology should be performed where possible. This approach has been used in the current research for modelling the tabular solids representing dykes when constructing a training image;

- Semi-deterministic approach such as distance-volume function for boundaries. An example of it is creating an RBF-based function when building a training image for BIF and diorite;
- Process-based model approach mimicking geological processes;
- Object-based modelling simulating geologic features of definite shape;
- Cell-based modelling techniques such as Sequential Indicator Simulation (SIS), Truncated Gaussain Simulation (TG) and MPS. The DS algorithm is just one of many among the MPS techniques.

The Direct Sampling multi-point algorithm employed in the lithology simulation proved to be fast and flexible. Many parameters are available to ensure good reproduction of the patterns found in the training image and good connectivity while maintaining global proportions of lithologies.

The irregularity of the interface between BIF and diorite lithologies demonstrated good reproducibility. There are no definite geologic object shapes, such interfaces are good-fit-for-purpose for cell-based techniques as MPS (Deutsch, 2013).

Difficulties were encountered when simulating dykes. Although in terms of final uncertainty assessment, reproducing the continuity of dykes was of negligible importance it was pursued for understanding the algorithm better and using it more effectively in future. A number of approaches were used to achieve this. Using an additional training image depicting large-scale morphology of dykes, showed to be promising. Imposing distance-based conditioning for the grid nodes in the vicinity of the drillholes, though not a holistically ideal approach, produced the most significant improvement.

One of the concerns common to cell-based techniques (Deutsch, 2013) and confirmed in the current research is that the simulated categorical variable proportions slightly depart from the target (input) proportions in an order of a few percent. In future, post-cleaning for noise removal can be used. While correcting deviating global proportions for each realisation it should preserve important connectivity.

Further improvement to the MPS simulation workflow can include the following:

- Hierarchical simulation of the lithologies (Deutsch, 2013). For simulation of more than three facies, it can improve the results. In the workflow, the main lithologies are simulated first, then secondary lithologies, followed by a “cookie-cutter” approach while sequentially expanding or eroding previous structures. It allows one to concentrate on one interface at a time, ensuring better inference from a training image. This approach was attempted when trying to use two different training images: for simulation of the host-rock and dykes and proved to produce good results;

- A unilateral path could be used for simulation of dykes, and stitched in a hierarchical fashion to the BIF and diorite lithologies mentioned above;
- Using diamond core structural readings to impose better control on the direction of the geological boundaries and to describe large scale stationary features will be geologically more "correct". It can also be used as a conditioning potential field for the gold simulation, incorporating locally varying anisotropy and trend modelling.

Some general considerations should be born in mind when performing simulation:

- Start with non-conditioned simulation until the pattern reproduction is good. The insufficiencies in parameters will come through in a main simulation where conditioning data is sparser;
- Test parameters and keep track of both – processing time and quality of reproduction using a common reference location for easier tractable comparison;
- It is recommended to use a grid with equal nodes spacing in all directions if visual validation of the results and reproduction of the spatial patterns is important;
- Rather use a generic training image and apply structural information if available for use on rotation and homothety. The TI should be as stationary as possible. Any manipulation should be presented in the form of potential fields images;
- It is important to have full scale features present in the training image, for example boudin-like compartmentalising of the host rock by dykes in the current project;
- Checking statistics for both continuous and categorical variables thoroughly in the early stage of simulation is important for validation of the performance to ensure reasonableness of the applied parameters and appropriate stationarity decisions;
- For processing large files some basic scripting knowledge is required even if commercial software is being used. The latter often has limitations on number of files, size of conditioning datasets, size of simulation grids, etc. Scripting will simplify many tasks;
- As anisotropy is borrowed from the training image, there will be short-scale continuity in the realisations and simulation results might present noise.

For the specific project, the following can be improved in the workflow:

- Stationarity domaining should be refined further, beyond the division in the three main lithologies. Sedimentary and chemical BIF populations should be simulated separately. Although they have been combined in the current project, the bi-modality of the gold distribution was reproduced well. The non-stationarity expressed in higher gold grades along the narrow shear zone should have been taken proper care of. This demonstrated itself in the poor reproduction of the diorite variograms. In future, a stochastic approach to ore domaining along the shear zone

can be undertaken. Nonetheless, the reproduciton of the shear zone was satisfactory. This will be further demonstrated in the next chapter;

- Using trend as an additonal input into the SGS will improve the continuity along the shear. Currently, it was only the anisotropy directions that defined the continuity of the high grade away from conditioning data.

The DS was applied to quite a simple pilot project in this study, and was limited to simulation of a categorical variable. The nature of mineralisation at Nyankanga lends itself very well to parametric description. The experimental variograms of gold look like typical 'text book' examples. It will be a good exercise in the future to use DS for simulation of both categorical and continuous variables. It can also be tested on a more complex mineralisation case, where variograms are not sufficient to describe the continuity or validate results. Care would need to be taken to produce a training image which would truthfully represent the small scale gold distribution.

4 POST-PROCESSING FOR UNCERTAINTY

4.1 Visualising uncertainty

Generation of multiple realisations gives an appreciation of the variability, assimilating it requires summarising to represent a joint uncertainty. A number of post-processing options for summarising both the lithology and grade realisations using GSLIB software were exploited. An emphasis in this chapter is given to assessing local rather than global uncertainty.

4.1.1 Post-processing lithology

The weighted average summary of all 50 realisations creates as an output a grid object with probability of each lithology type, a most likely to occur lithology and entropy. The examples are shown in Figure 4.1.

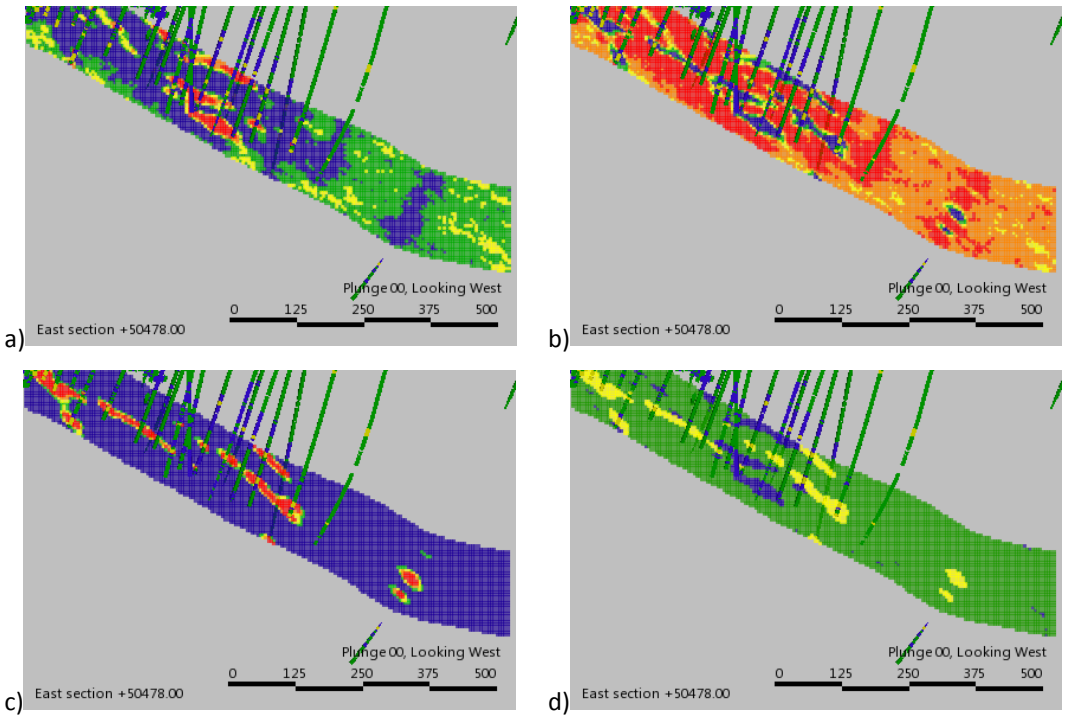

Figure 4.1. Summary of the post-processing output of lithology simulation.
a) probability of BIF, b) probability of diorite, c) probability of quartz porphyry, d) the most likely to occur lithology type.

Post-processing for the most-likely to occur lithologies would be similar to a result of indicator kriging.

Entropy introduced by Christakos (1990) represents a measure of uncertainty in a probability distribution function (Deutsch, 2013). As can be seen in Figure 4.2, the lower entropy values are observed in the vicinity of the drillholes, where the continuity allows determination of the conditional probabilities with high confidence. The highest entropy can be seen on the peripheries of the most-likely dykes' boundary, as this is the lithology with the most uncertainty in the study.

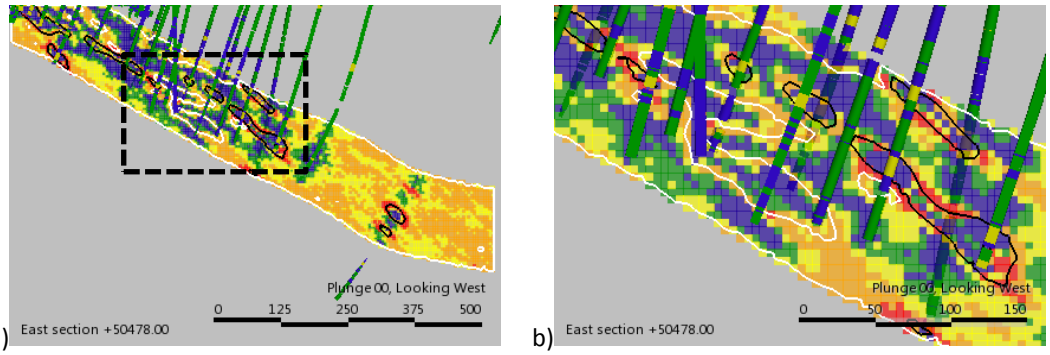

Figure 4.2. Entropy for lithology simulations.
a) N-S sectional view of the simulated grid, b) 'zoomed-in' area of the section.

4.1.2 Post-processing grade

The simulated uncertainty of the gold distribution is inclusive of the uncertainty of lithology.

The maps of the conditional variance and the expected mean for all 50 realisations are shown in Figure 4.3. They demonstrate a strong dependency between the local mean and the conditional variance. The proportional effect is common for positively skewed distributions. It expresses itself as high-grade areas having a greater variability, hence uncertainty, than the low-grade areas. For lognormal distributions, the local standard deviation is proportional to the local mean (Journel and Huijbregts, 1978).

Reproduction of the higher-grade shear zone is very good even without the ore grade domaining or a structural trend. Away from the conditioning data, as can be seen in the bottom left corner of the Fig.4.3, the gold distribution follows the planar direction of the variogram.

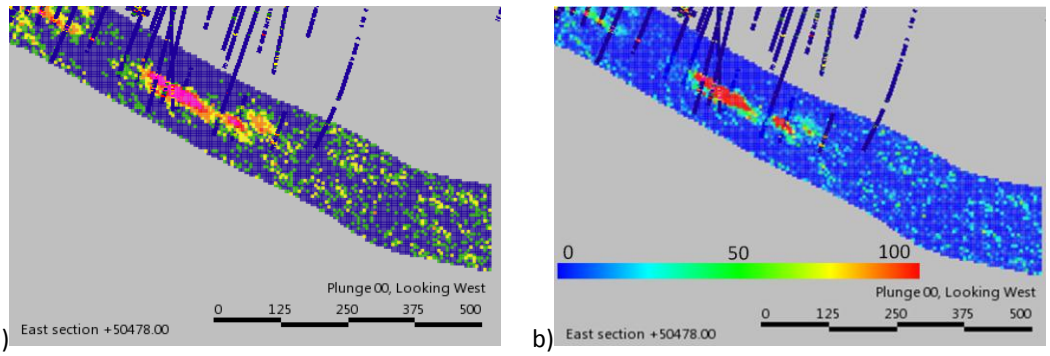

Figure 4.3. Post-processing results of the E-type averaging of the gold simulation, sectional view.
a) E-type mean of the 50 realisations, b) conditional variance of the 50 realisations,

In Figure 4.4, the results of the post-processing for a specific grade cut-off are shown. For an easier analysis, the wireframes representing the most likely lithology are also displayed. Once again, a poor decision on stationarity demonstrates itself in smearing of high grade values across the simulation volume in the absence of conditioning data. For future work, high-grade domaining along the shear should be used.

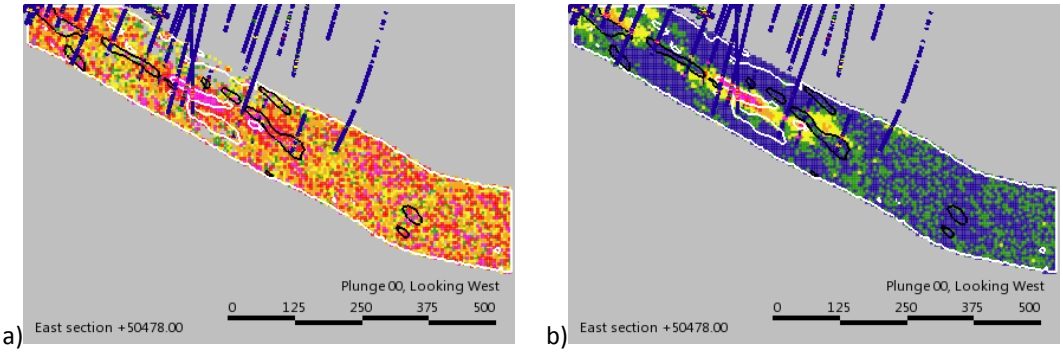

Figure 4.4. Post processing for a selected cut-off grade, sectional view.
a) average grade above the cut-off, b) probability being above the cut-off grade.
The solid outlines represent the most likely lithology types: black – interface between the quartz porphyry dykes and host rock, white – interface between the BIF and diorite.

An example of post-processing of the specified probability interval to be within a relative error of the mean is shown in Figure 4.5. The probability of 90% can be observed only in the vicinity of the drillholes. This is due to short scale variogram ranges. Areas of higher drilling density, as in the top left corner of Figure 4.5b, have less uncertainty.

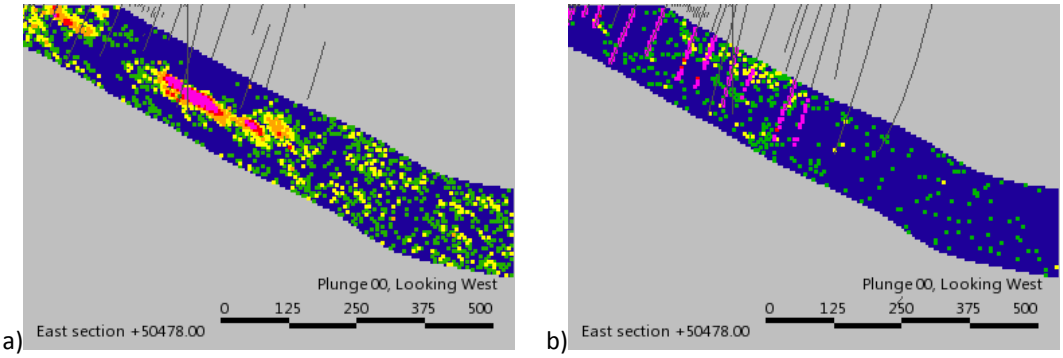

Figure 4.5. Post-processing results of probability of being within 15% error of the Au E-type mean, sectional view.
a) E-type mean of the 50 realisations, b) probability of being within 15% error of the mean.

On Figure 4.6, different percentiles of being within the estimated E-type mean are displayed. The P10 (Figure 4.6a) and P90 (Figure 4.6c) show the symmetric 80% probability interval around the E-type mean. The areas which are certainly high in relation to the mean show as high-grade on the lower limit P10 map. On the P90 map, low values are indicative of areas with certainly low grade. The P50 map represents the most likely outcome.

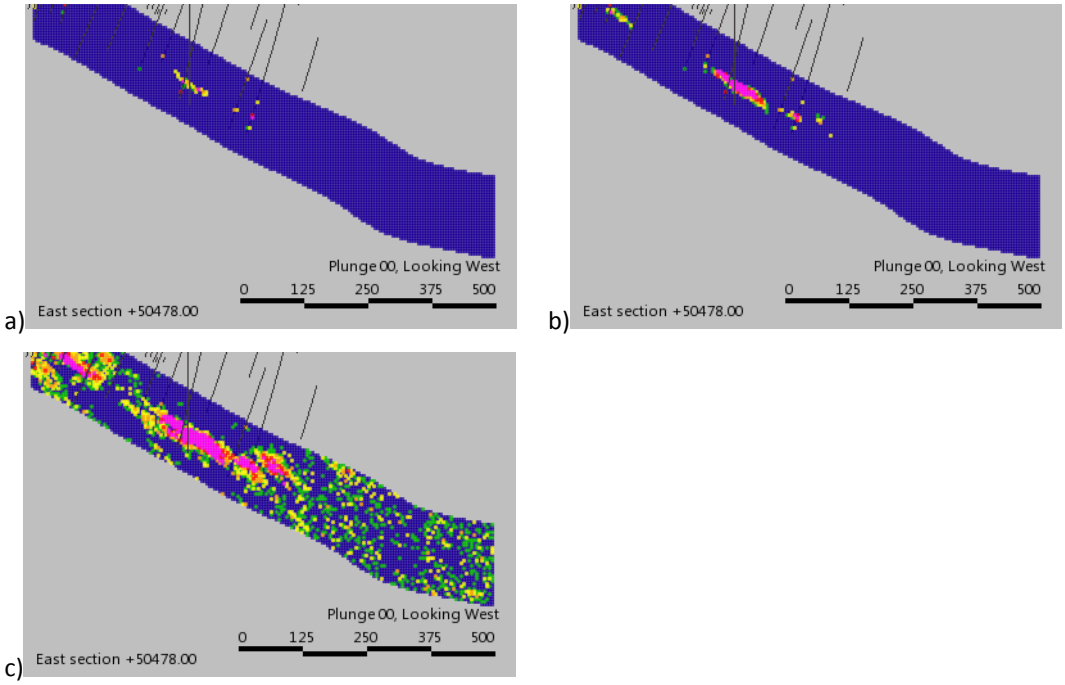

Figure 4.6. Probability of being above a specified cut-off grade.
a) P10 percentile; b) P50; c) P90.

The final comparison performed for the study clearly demonstrates one of the main findings of the research – the importance of the stationarity assumption in the simulation. In Figure 4.7, an E-type average of the 50 gold realisations is displayed together with the drillhole samples available over the Nyankanga deposit. While the reproduction of the high-grade shoots orientation is in coherence with the picture demonstrated by the samples, the low grade values in the simulation are much higher than the background low grade values of the area seen from the drillhole samples. Note: yellow background in the simulation grid versus royal blue background of the drillhole samples (Figure 4.7).

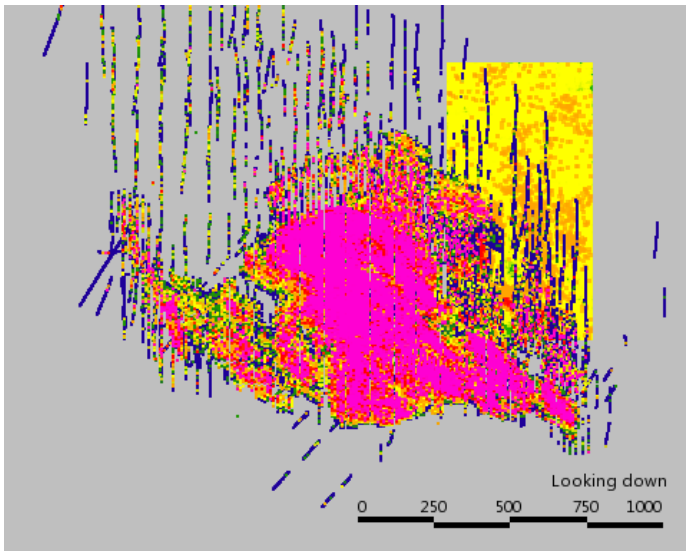

Figure 4.7. Plan view of the Nyankanga deposit showing the simulation grid with the drillhole samples.

The importance of the stationarity in geostatistics has been emphasized numerous times, and it is vividly demonstrated here. As stated by Caers (2002:5): “The multi-variate Gaussianity by definition generates reservoir models that are ‘homogeneously heterogeneous’... Amongst all possible reservoir models that reproduce a given variogram.., SGS generates models that are maximally disconnected in the low and high values. This property of SGS is also termed the ‘maximum entropy’ property.”

4.2 Block averaging to recoverable resources

Scaling the realisations up makes the uncertainty conclusions meaningful for a specific purpose. Upscaling fine resolution realisations to grid nodes of a panel size can be used for further processing in the mine planning process, upscaling to a SMU size can be used to assess uncertainty in mine scheduling process.

For the variables involved in the estimation of the mineral resources, such as concentration of minerals and densities of rocktypes, averaging to a larger support size is linear. It means that for continuous variables the mean stays constant within the volume being upscaled, for categorical variables - the most probable lithology is assigned to larger size blocks by volume weighting. It would not be the case for non-linear averaging variables (Journel, 1996), such as geometallurgical parameters or rock permeability.

Smoothing in the variables and uncertainty takes place during upscaling. This effect can be seen in Figure 4.8 which shows the fine–resolution simulation of 5m nodes spacing (Figure 4.8a, b) and a version upscaled to nodes spacing of 40mE x 40mN x 10mElev (Figure 4.8c, d). Large variability observed at small scale is considerably smoothed at large scale nodes.

The upscaled realisations can be processed to generate grade tonnage curves to get a representation of uncertainty in the recoverable metal.

The mining optimisation should be performed for all upscaled realisations. It can also be done for a few selected ones which can be chosen based on different transfer functions or performance calculations (Deutsch, 2013), such as metal content or degree of “connectivity” of the panel blocks above a chosen grade cut-off. In this case, the scenarios can be a P50 percentile which would represent a base case, and the P10 and P90 percentiles.

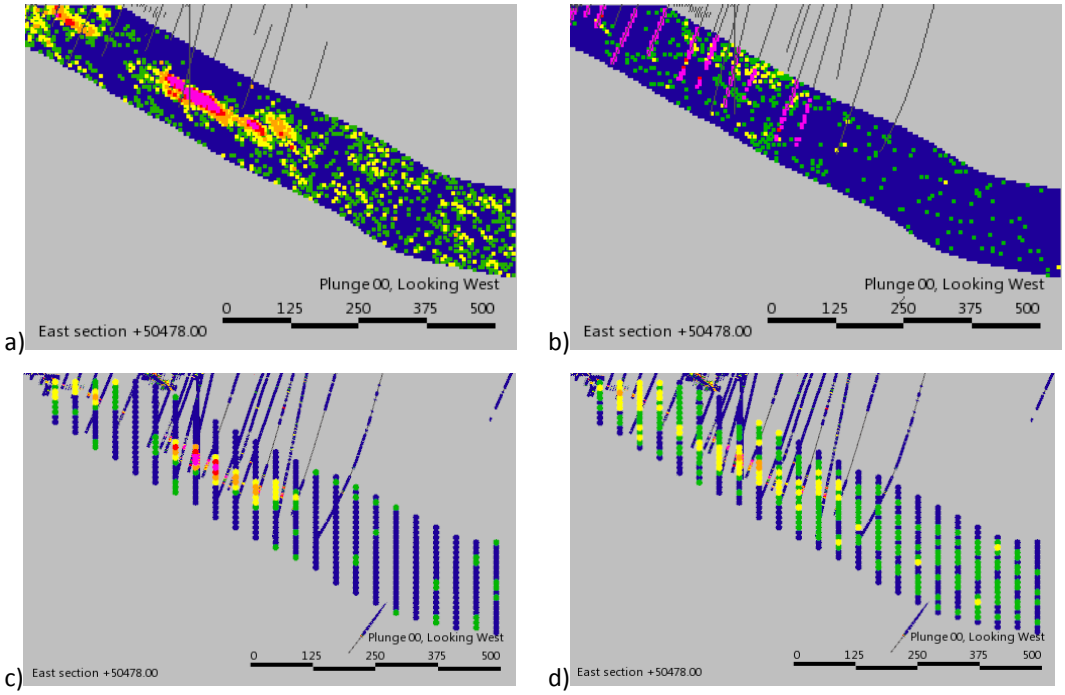

Figure 4.8. An upscaled simulated model: probability of being within 15% error of the Au E-type mean, sectional view.
a) E-type mean of the 50 fine realisations, and b) probability of being within 15% error, grid of 5m x 5m x 5m node spacing, c) E-type mean of the 50 upscaled realisations, and d) probability of being within 15% error, grid of 40m x 40m x 10m node spacing. In the course resolution grid, spheres represent grid nodes.

4.3 Comparison to a kriged model

The realisations upscaled to a panel size were further compared to a kriged model to get a feel of the uncertainty associated with a deterministic approach to estimation.

The kriged model with the cell size of 40mE x 40mN x 10mElev contains the two main lithologies, BIF and diorite, estimated by indicator-kriging with the resulting volumetric proportions assigned to each cell.

For the simulated model, average densities were used during the upscaling process: 3.05g/t for BIF and 2.72g/t for the felsic intrusives.

The comparison was done within a deterministically interpreted volume representing ore along the shear zone to eliminate the effect of inadequate stationarity domaining in gold simulation. The extent of the volume is shown in Figure 4.9.

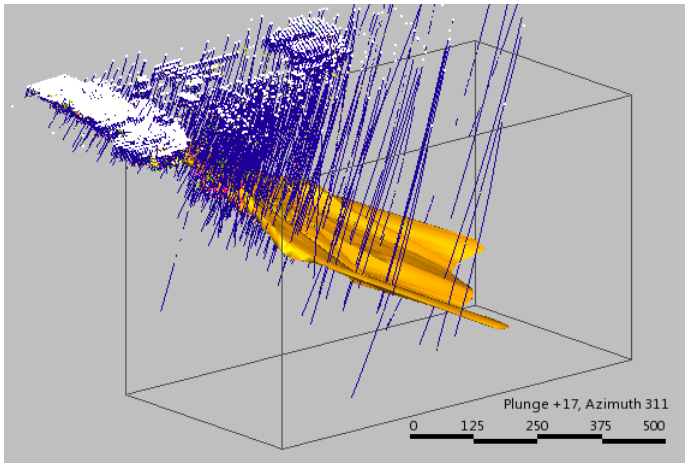

Figure 4.9. Deterministically interpreted volume of the ore along the shear zone used for comparison of the kriged model and simulation results.

The histograms of the gold grade within the common volume are presented in Figure 4.10. They are based on the cell centroids falling within the volume of ore. Although no direct comparison for accuracy or method precision could be performed due to the fact that a different algorithm was used in the kriging (slightly different source data, differing capping strategy, decisions on stationarity and models of spatial correlation), some global comparisons have been made. Note, the gold statistics presented in this chapter have been factorised.

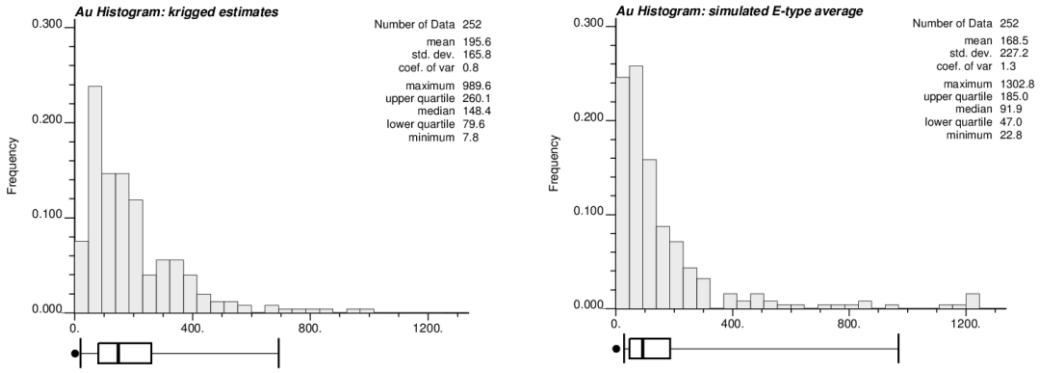

Figure 4.10. Histograms of the kriged and simulated E-type average of gold at panel size blocks, compared within a common volume.
a) kriged estimates, b) simulated E-type average of 50 realisations.

The gold histograms shown in Figure 4.10 demonstrate a well-known truth: the kriged estimates are too smooth. The interquartile range which is a measure of the spread of a distribution is smaller in the simulated average model than in the kriged model. The mean and median are also considerably lower.

Figure 4.11 shows the two models side by side: on the left – the kriged model within the ore wireframe, on the right – the averaged result of the 50 realisations. In the well informed areas, the two approaches demonstrate closely correlated results in the gold values, with less smoothing observed in the simulated model.

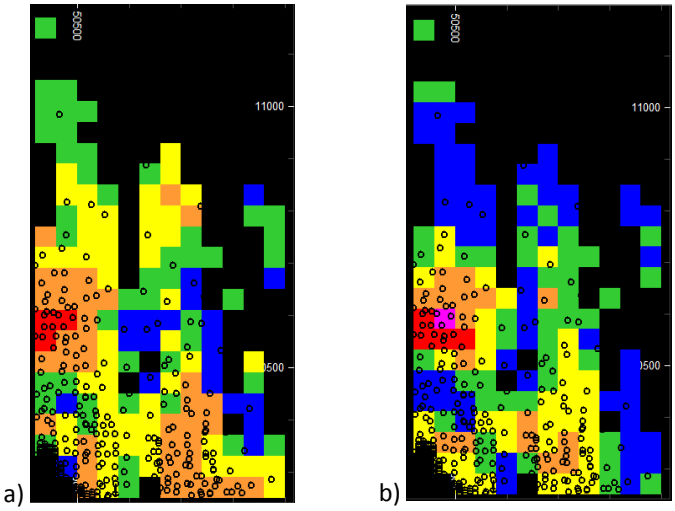

Figure 4.11. Comparison of the kriged and simulated gold grade for the cells falling within the shear zone.
a) kriged block model portion, b) average of 50 realisations, upscaled to 40m x 40m x 10m cell size.
The black circles represent drillhole samples intersecting the ore wireframe.

Comparison of the density histograms for the models is shown in Figure 4.12. In the simulations, the overall global proportions of the lithologies are representative of the conditioning data. The distribution is positively skewed reflecting the higher proportion of the felsic intrusives. In the kriged model, the density distribution shows smearing of values towards the higher end which is indicative of the larger proportion of BIF. The average density of the kriged model within the common ore volume is higher than for the simulation, 2.80g/cm^3 for kriging versus 2.76g/cm^3 for the simulation average.

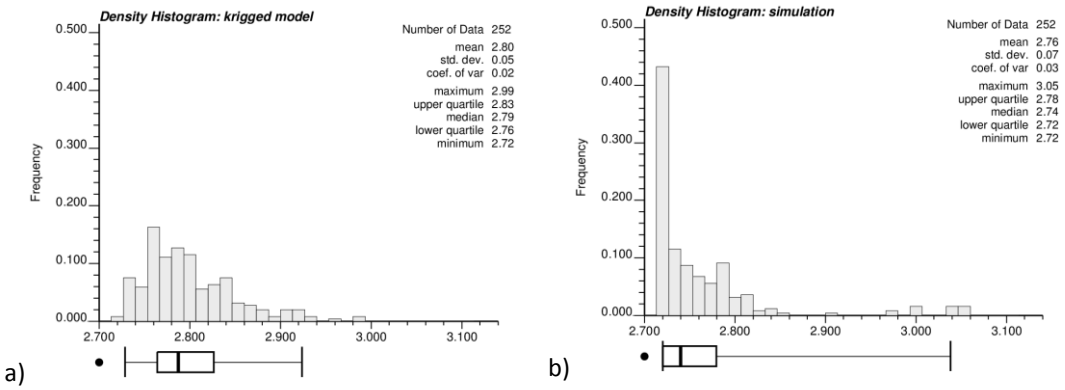

Figure 4.12. Histograms of the densities assigned to the kriged model and simulated realisations, compared within a common volume.
a) kriged model density; b) simulation model density.

A plan view of the two models in Figure 4.13 demonstrates the spatial prevalence of the lower density felsics in the simulated model and favouring of the BIF units in the kriged model.

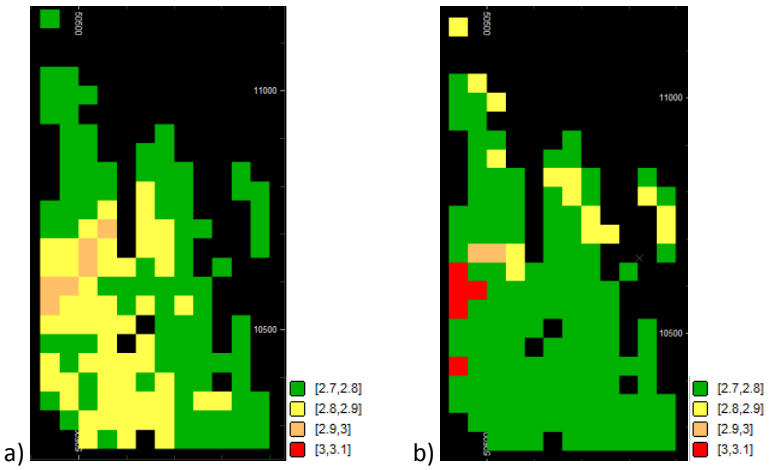

Figure 4.13. Comparison of the densities in the kriged and simulated model cells falling within the shear zone. a) kriged block model, b) average of realisations, upscaled to 40m x 40m x 10m cell size.

Figure 4.14 displays scatterplots of the gold and density values within the common ore volume compared on a block by block basis. For the gold (Figure 4.14a), the simulated model shows presence of extreme values which represents the input distribution more truthfully. The correlation coefficient of 0.82 expresses a good correlation between the two methods. Overall, the scatter between the two models is considerable and it gets more pronounced for the high grade cells. Two distinct areas are observed on the scatterplot: for the range of values 0-400 units the kriged model contains higher grades than the average of simulations, above the threshold of 400 the reverse is true.

The scatter of block densities on a block by block basis is wide, the correlation is positive. The distribution of density values in the simulated model shows presence of blocks with purely diorite or BIF lithologies. The kriged model within the common volume contains small portions of blocks composed of single lithology. It can be explained by the fact that the indicator kriging used to estimate the lithologies in the kriged model was based on a longer range variogram established from widely spaced drilling, while the simulation replicates short scale variability between the BIF and diorite observed in the training image.

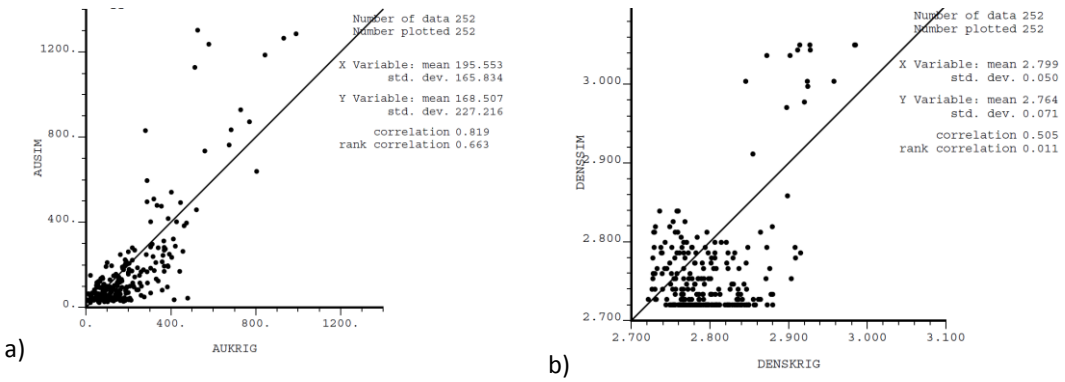

Figure 4.14. Scatterplots of gold and density for simulated vs kriged model. a) gold; b) density.

4.4 Discussion

A brief introduction to ways of assessing uncertainty was demonstrated in the chapter.

Most of us comprehend concepts visually, visualisation of the results by post-processing the stochastic models provide a good presentation of uncertainty.

A comparison to a kriged block model confirmed a well-known truth that kriging, while being the "best linear unbiased estimate", creates an over-smoothed model of reality.

Some further improvements to the workflow can be considered (Deutsch, 2013):

- Realisations can be processed through a transfer function or performance calculation. In the context of mining it can be a grade-tonnage curve, degree of connectivity of the ore/waste blocks, or mine scheduling;
- Realisations may be ranked to select a few for detailed processing;
- Scenarios and parameter uncertainty is important. For assessing it, the realisations can be sampled with Monte Carlo Simulation or Latin Hypercube Sampling;
- Currently, processing of multiple geostatistical scenarios is "intractable" in the mine planning and scheduling practice (Deutsch, 2013). At the same time, using one deterministic scenario, whether a kriged model or a realisation can lead to "overplanning" on a stochastic feature. Optimisation must be performed with all realisations simultaneously.

The value of stochastic approach to modelling is that it provides an appreciation of the extent of uncertainty when making an appropriate decision. On the other hand, it is also possible to average outcomes of many realisations and produce a smoothed result which is very close to kriging.

High-resolution simulation grids cannot be used efficiently. They should be upscaled to coarser resolution of SMU size and panel size to make assessment of uncertainty more meaningful.

There are a few considerations which must be born in mind with regards to uncertainty assessment (Deutsch, 2013):

- Uncertainty assessment is model-dependant and stationarity dependant. Improper stationarity decisions result in higher uncertainty. This statement was very well unintentionally demonstrated in the study;
- Many parameters affect the distribution of uncertainty in a non-intuitive and non-transparent manner;
- Uncertainty in the histogram and spatial continuity can have a large effect on the large mining-scale uncertainty;

- Quantitative uncertainty, e.g. probability to be within +-15% with 90% confidence, should be used to support geometric criteria for classifying reserves and resources. In this way, probabilistic meaning will enhance classification and make it easier to understand for a non-specialist.
- The uncertainty assessment is often not intuitive. Gold mineralisation is characterised by skewed distributions and proportional effect. The increased variability in the extreme values spreads uncertainty response. Larger proportions of low values are associated with low uncertainty. Spatial correlation plays a big role: poor spatial correlation causes increase in uncertainty, and the opposite is true.

5 CONCLUSION AND RECOMMENDATIONS

5.1 Summary of findings

In the current research an attempt has been made at utilising an MPS simulation approach for generating realisations of mineralised units, combined with a traditional SGS simulation of grade. The uncertainty of the lithology and grade simulations has been analysed. Some examples of uncertainty assessments have been presented to demonstrate that the amount of information provided by stochastic simulations is an order of magnitude richer than a kriged model can provide.

The Direct Sampling approach has shown to be flexible and robust. The possibility of running it in multi-core mode fully utilising the resources available on a particular pc, makes it competitive with many other commercially available algorithms.

Considering the scale of modelling when creating a training image and deciding on the grid resolution is important. The scale at which uncertainty assessment is taking place must be considered. For example: size of lithological units in comparison to the scale at which the decision will be made - SMU or panel size.

The choice of tools to be employed for a particular model is determined by the objective at hand. It should always be in a favour of simplicity and effectiveness. In the presence of a high data density and low uncertainty in the geological setting, a deterministic approach should prevail. An MPS method should be employed when a conventional parametric description would compromise a truthful representation of the natural phenomena. Pro's and con's should be weighted before undertaking this approach. In the current research, a traditional algorithm as Sequential Indicator Simulation would have probably yielded sufficiently good and similar results for simulation of the BIF and diorite lithologies. It would have however failed at reproducing the morphology of dykes. Considerable time has been spent on getting the reproducibility of the latter right, for the purpose of future usability.

Stochastic modelling and an MPS method in particular do not lighten the amount of technical work and computing power required. Time to produce such a model is not less than via conventional approach. Data preparation and analysis, results validation and post-processing take the major bulk of time. However, acceptance or rejection of a training image is more visual than a parametric model. It can be more inviting for involvement of specialist geological expertise, besides geostatisticians, and would provide more integration of different skills and ownership for field geologists.

5.2 Recommendations for a future use of an MPS approach

A particular care needs to be taken when choosing a training image. It is the training image which carries the decision on stationarity and geological settings to be simulated over the entire volume of interest. The best approach is to have a stationary training image, and deal with any non-stationarity by the means of trends or potential fields for homothety and rotation. Local proportions of categories can provide further control on the trend.

Sufficient repetition needs to be present in the training image to avoid an effect of "patching". Reproduction of large scale patterns would require a training image which contains them.

Hierarchical approach to lithology simulation can be explored in future. Multiple training images for different lithologies and different scale features will be useful.

5.3 General recommendations on stochastic modelling workflow

A stochastic approach carries a heavy reliance on the condition of stationarity. It is not explicitly obvious in Sequential Gaussian Simulation, but is expressed under the condition of multi-variate Gaussianity. The effect of making a stationarity omission during simulation is more unforgiving than for example with the ordinary kriging (Deutsch, 2013). Analysing the data and geological settings to make an appropriate decision on stationarity is crucial for valid uncertainty statements. Such a workflow would involve:

- Reviewing geological model, contacts and large scale trends;
- Deciding on the modelling scale;
- Reviewing statistics and spatial correlation in different geological units;
- Taking care in defining stationary domains;
- Evaluating appropriate measure of uncertainty for analysis;
- Considering multiple realisations to quantify the current state of uncertainty;
- Relating uncertainty to drillholes spacing;
- Performing sensitivity analysis to understand how parameter uncertainty and choice of uncertainty measures affects the results;
- Documenting the methodology, results and recommendations.

5.4 Recommendations for future work

The Direct Sampling algorithm was applied to quite a simple case in this study, and was limited to simulation of a categorical variable. The nature of mineralisation at Nyankanga yields itself well to parametric description. The experimental variograms seems to have been borrowed

from text books. The DS should be tested on a more complex mineralisation case, where variograms are not sufficient to describe the continuity and hence to validate the result. The gold mineralisation is almost always structurally controlled. Structures cannot be effectively described by a variogram.

There is a scope for future work to test applicability of DS for simulation of categorical and continuous variables simultaneously. Prior to undertaking it, care will have to be taken to produce a training image truly representative of mineralisation.

Using an additional control in the form of drillhole structural readings can enrich the realness of the resulting model. It can be used in different ways: as an additional control on the interface between different rock types, or in reproducing the morphology of the large scale intrusive units and structures.

A richness of high resolution expensive data is obtained from diamond core drilling. An enormous amount of specialist time goes into collecting and interpreting it. Examples include structural core logging or core scanning imaging, the latter represents new advances in technology. Unfortunately, in the most cases, it does not get utilised to the full extent. This information could be incorporated to produce more informed training images or to provide additional “soft” conditioning and potential field grids for manipulating size, rotation and attitude of the training image patterns. Using this data would allow one to go beyond inferring training images from outcrops and be used in both large and small scale modelling and uncertainty assessment.

Other possible uses of the DS algorithm can include simulating poorly informed sections of otherwise well informed area using the restoring capability of the DS.

There is still a big gap between the implementation of any algorithm for research purposes and its practical use. Many questions about the use of multiple-point geostatistics remain open, particularly related to the choice of a training image, model construction and validation.

6 REFERENCES

Brayshaw, M., Nugus, M., Robins, S. (2010) *"Reassessment of controls on the gold mineralisation in the Nyankanga deposit – Geita Gold Mines, North-Western Tanzania."* Paper presented at the 8th International Mining Geology Conference, Queenstown, New Zealand, August 21-24, 2011.

Caers, J. (2011) *"Modelling uncertainty in the Earth Sciences"*. Published by Wiley-Blackwell, Ltd. pp 90-106.

Caers, J., Zhang, T. (2002) *"Multiple-point geostatistics: a quantitative vehicle for integrating geologic analogs into multiple reservoir models"*. Stanford University Press, Stanford Center for Reservoir Forecasting, Stanford, CA 94305-2220.

Comunian, A., Renard, P. (2011) *"Probability aggregation methods and multiple-point statistics for 3D modeling of aquifer heterogeneity from 2D training images"*. Thèse de doctorat, Université de Neuchâtel, Switzerland.

Deutsch, C., Journel, A. (1998) *"GSLIB: Geostatistical Software Library and User's Guide, Second Edition".* Oxford University Press, Oxford.

Deutsch, C. (2013) *Lectures on Citation Program in Applied Geostatistics, presented in Johannesburg, RSA*. Centre for Computational Geostatistics. University of Alberta, Edmonton, Alberta, Canada.

Emery, X., Ortiz, J., Rodriguez, J. (2006) *"Quantifying Uncertainty in Mineral Resources by Use of Classification Schemes and Conditional Simulations".* Mathematical Geology, Vol. 38, No 4, May 2006, pp 445-464.

Geita Gold Mine. (2013) *"Resource Model Handover Note for Nyankanga Gold Deposit".* AngloGold Ashanti internal reporting.

Guardiano, F., Srivastava, R., (1993) *"Multivariate geostatistics: beyond bivariate moments"*. Quantitative Geology and Seostatistics, Vol. 5, pp 133-144.

Jones, P., · Douglas, I.,· Jewbali, A. (2013) *"Modeling Combined Geological and Grade Uncertainty: Application of Multiple-Point Simulation at the Apensu Gold Deposit, Ghana".* Mathematical Geosciences, Vol. 45, Issue 8, pp 949-965.

Journel, A., Huijbregts, C. (1978) *"Mining Geostatistics".* Academic Press, p 187.

Journel, A. (1996) *"Conditional simulation of geologically averaged block permeabilities*." Journal of Hydrology. Vol. 183, no 23, p 23.

McLennan, J., Deutsch, C., DiMarchi, J., Rolley, P. (2004) *"Geostatistical Determination of Production Uncertainty: Application to Pogo Gold Project"*. Canadian Institute of Mining, Edmonton.

Meerschman, E., Pirot G., Mariethoz, G., Straubhaar, J., Van Meirvenne, M., Renard, P. (2012) *"Guidelines to Perform Multiple-Point Statistical Simulations with the Direct Sampling Algorithm"*. Ninth International Geostatistics Congress, Oslo, Norway, June 11 – 15, 2012.

Meerschman, E., Pirot, G., Mariethoz, G., Straubhaar, J., Van Meirvenne, M., Renard, P. (2013) "*A practical guide to performing multiple-point statistical simulations with the Direct Sampling algorithm".* Computer & Geosciences, Vol.52, pp 307-324.

Perez, C., Ortiz, J. (2011) *"Mine-scale modeling of lithologies with multipoint geostatistical simulation"*. IAMG, University of Salzburg publication, September 5-9.

Remy, N., Boucher, A., Wu, J. (2009) *"Applied Geostatistics with SGeMS"*. Cambridge University Press.

Rezaee, H., Mariethoz, G., Koneshloo, M., Asghari, O. (2013) *"Multiple-Point Geostatistical Simulation Using the Bunch-Pasting Direct Sampling Method"*. Computers and Geosciences, Vol.54, April 2013, pp 293-308.

Tahmasebi, P., Hezarkhani, A., Sahimi, M. (2012) *"Multiple-point geostatistical modelling based on the cross-correlation functions"*. Computational Geosciences, Vol.16, Issue 3, June 2012, pp 779-797.

Yunsel, T. (2012) *"Risk quantification in grade variability of gold deposits using Sequential Gaussian Simulation"*. Journal of Central South University, Vol.19, Issue 11, November 2012, pp 3244-3255.

http://en.wikipedia.org/wiki/Monte_Carlo_method. Cited on 30 November 2013.

http://wiki.artofproblemsolving.com. Cited on 28 November.

7 APPENDICES

Appendix A: Variograms of the conditioning drillhole samples within the training image

Variograms for lithological interface between BIF and diorite

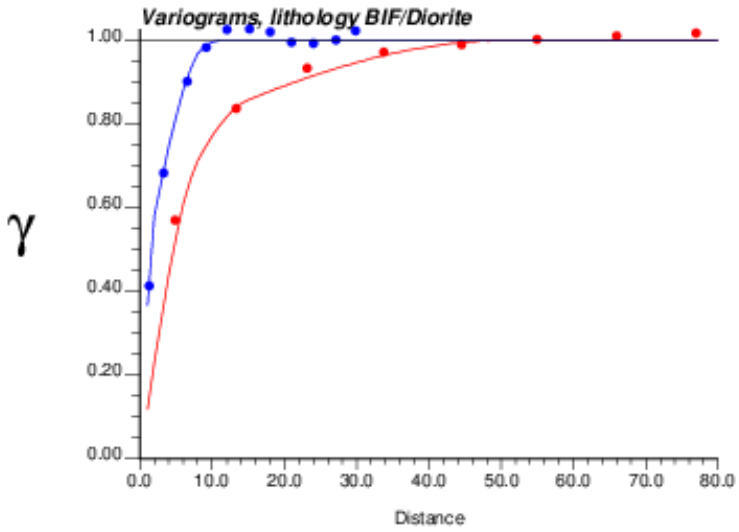

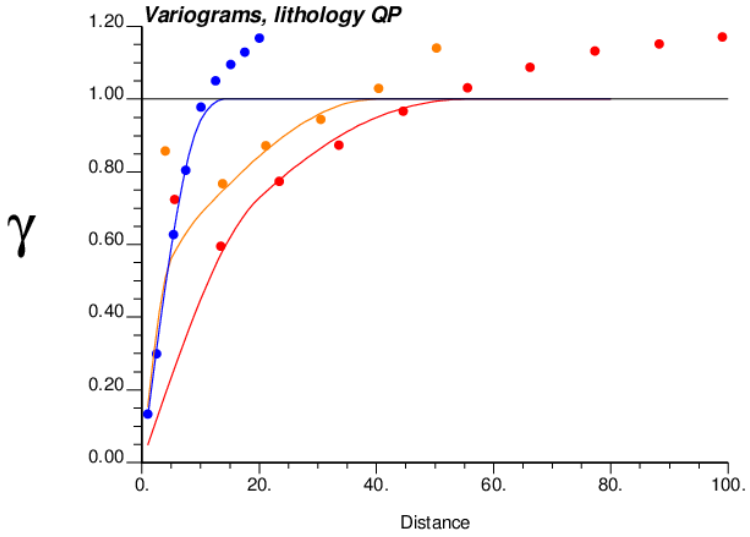

Gold variograms for BIF in original space

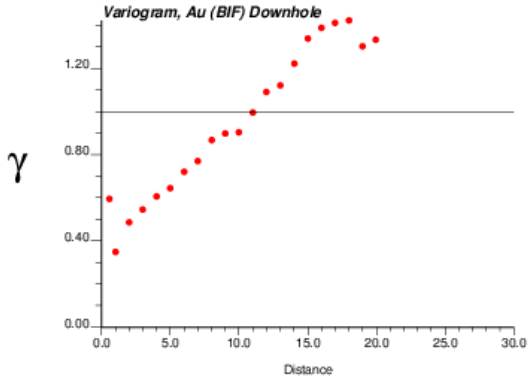

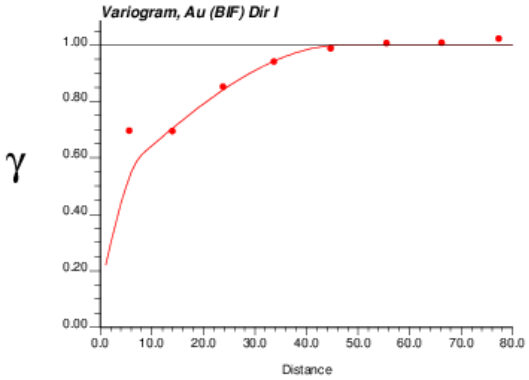

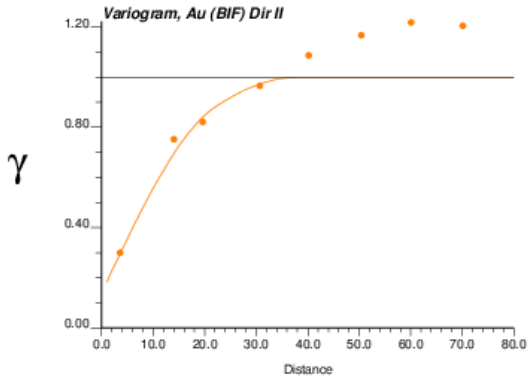

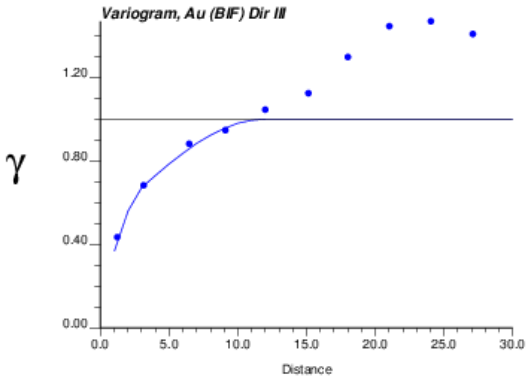

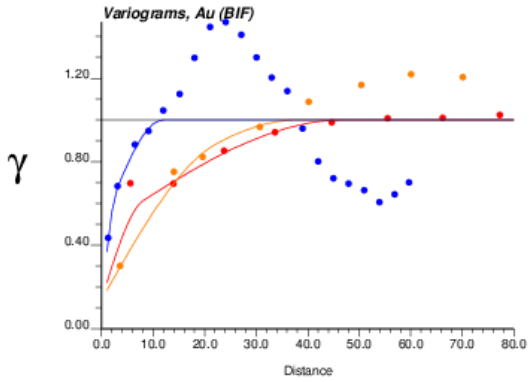

Gold variograms for BIF in Gaussian space

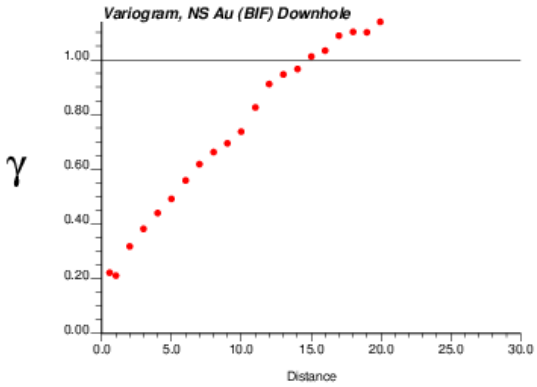

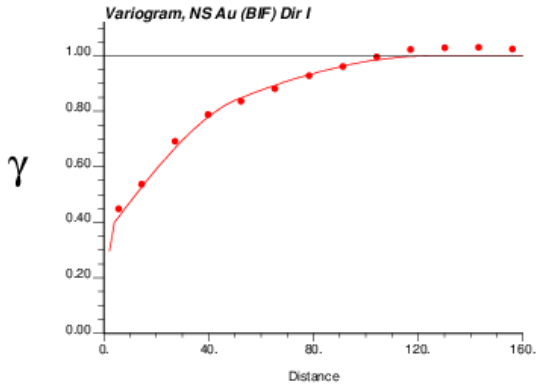

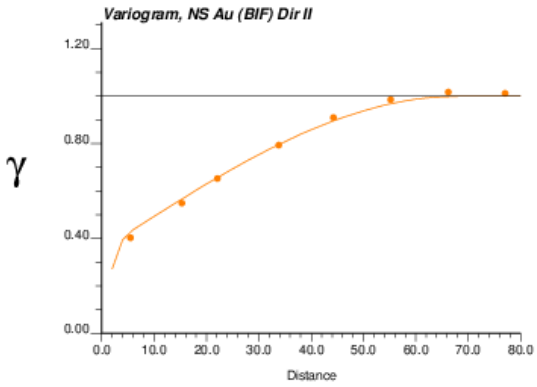

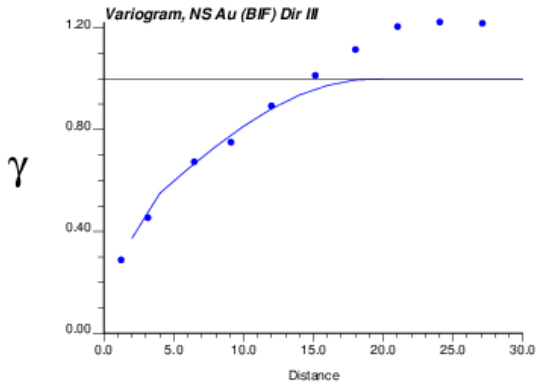

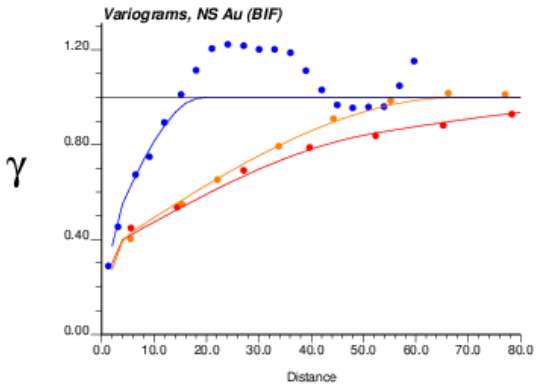

Gold variograms for Diorite in the original space

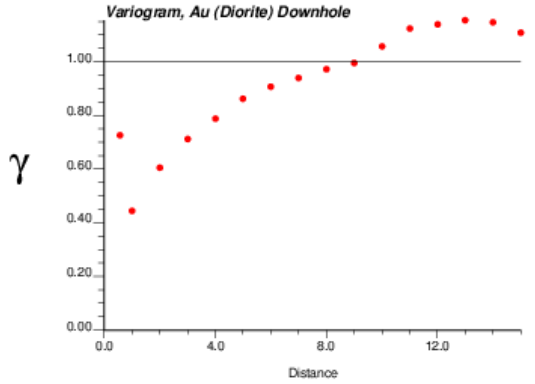

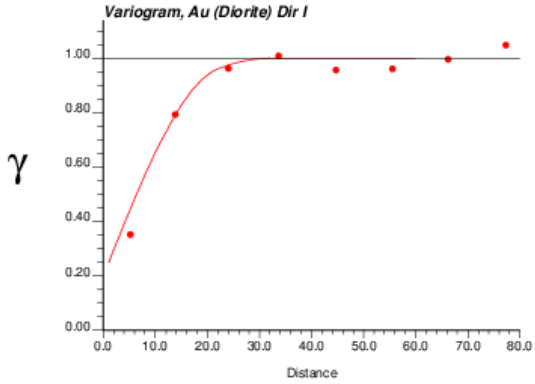

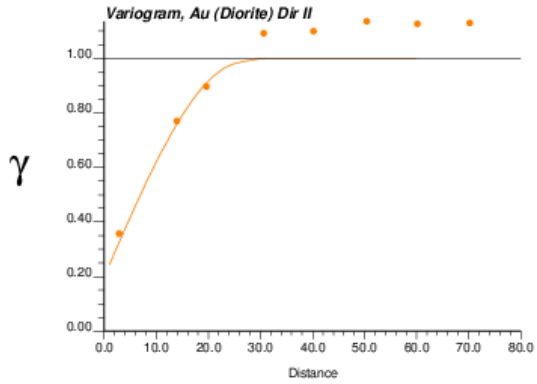

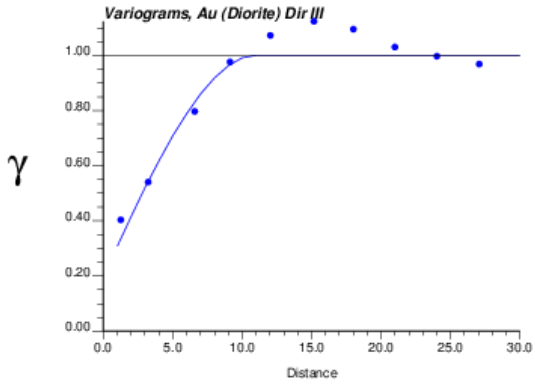

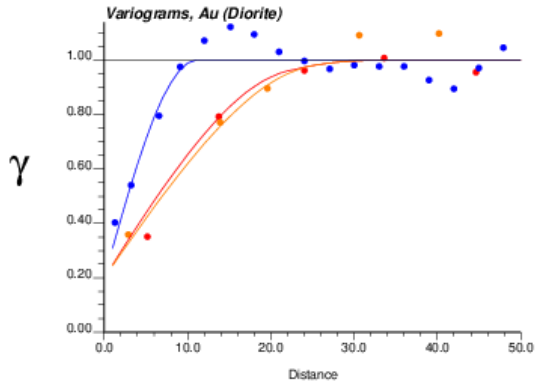

Gold variograms for Diorite in Gaussian space

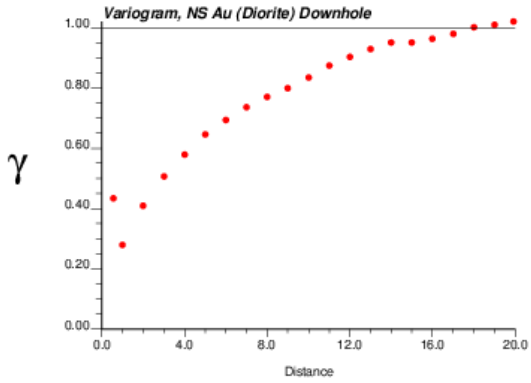

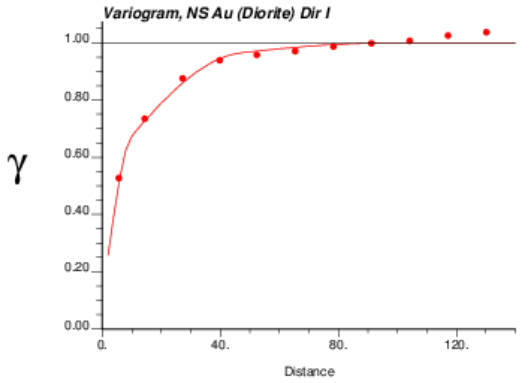

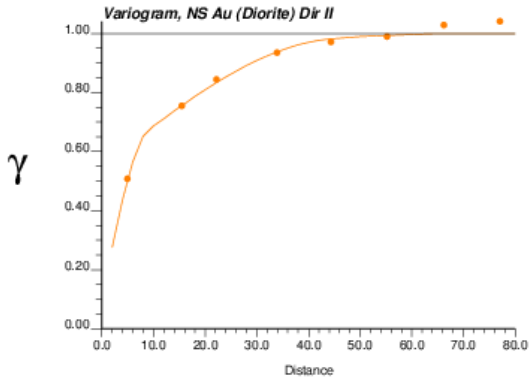

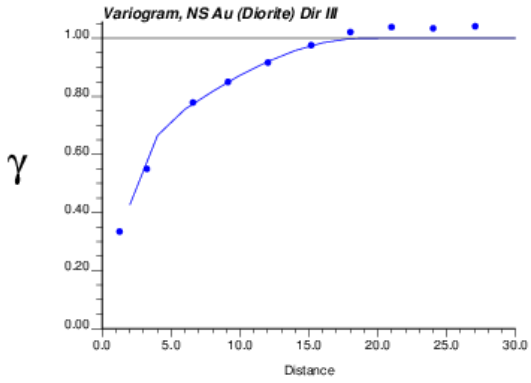

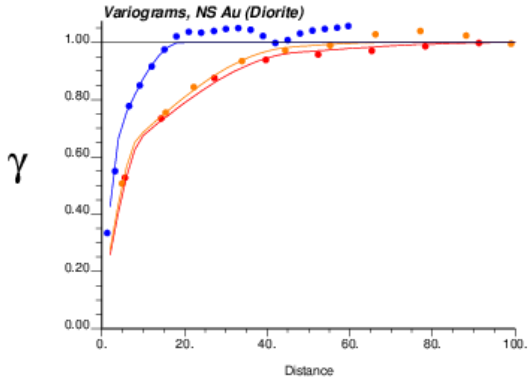

Gold variograms for quartz porphyry in original space

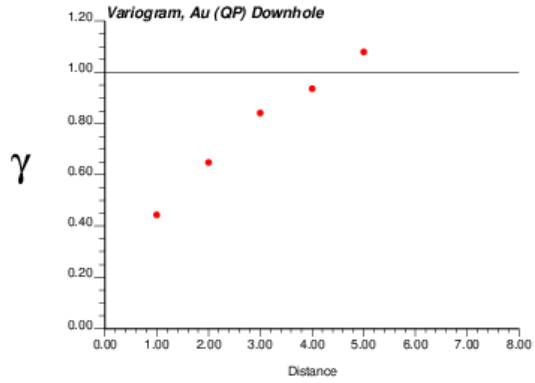

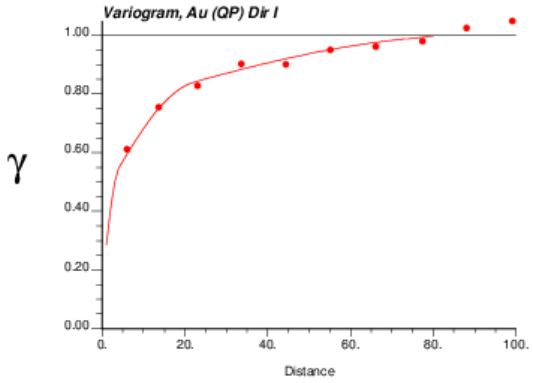

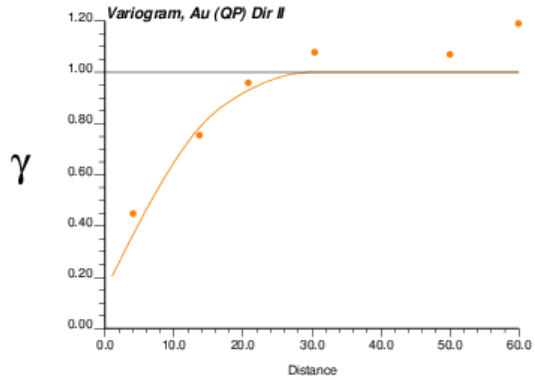

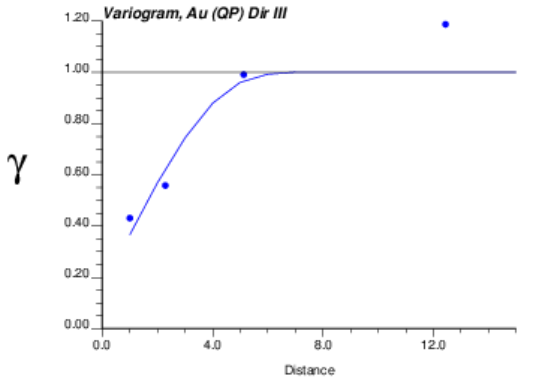

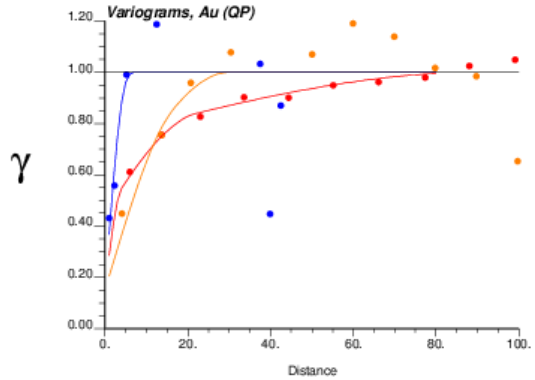

Gold variograms for quartz porphyry in Gaussian space

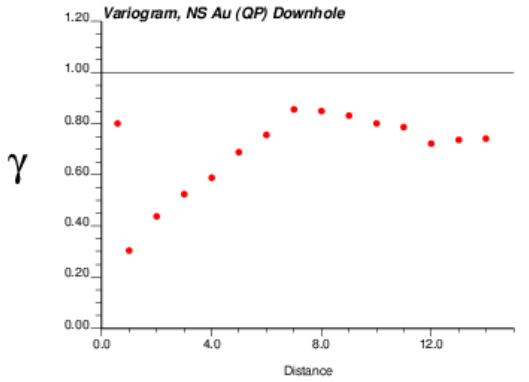

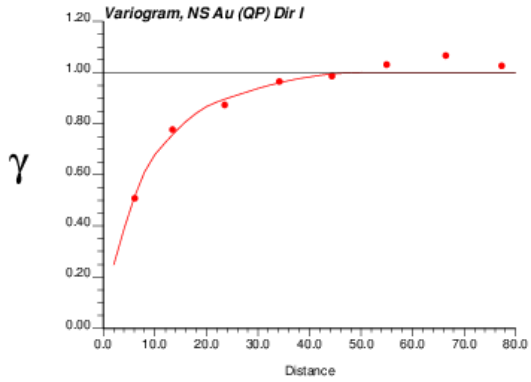

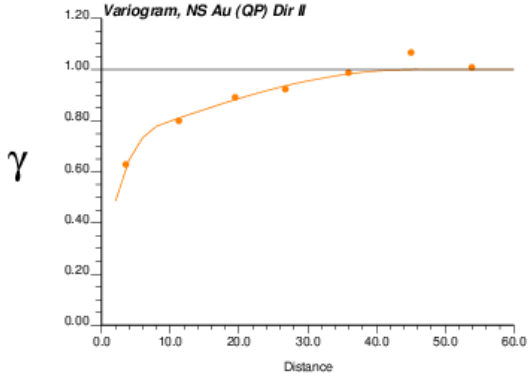

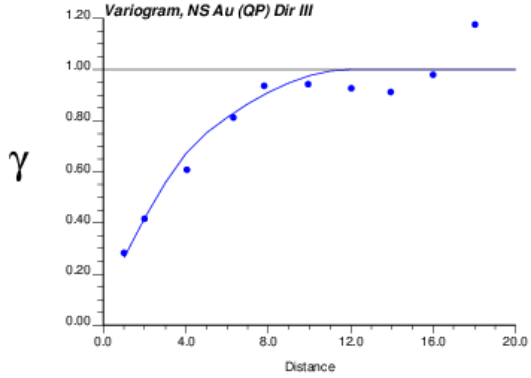

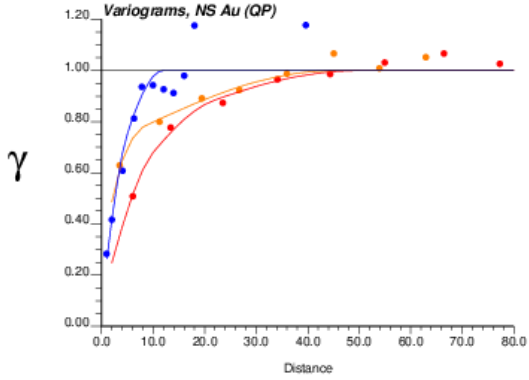

Appendix B: Variograms of the Sequential Gaussian Simulation results within the training image

Variograms for gold simulation in BIF

a) Variograms along easting; b) variograms along northing; c) variograms along elevation

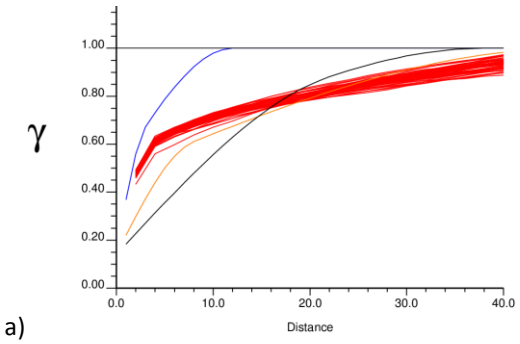

a)

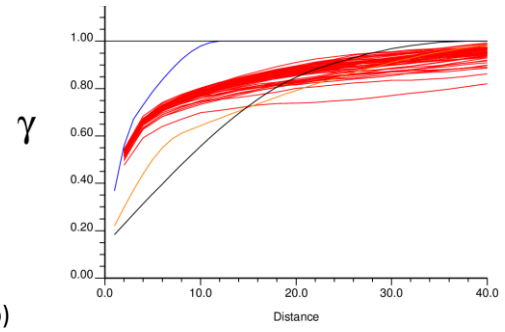

b)

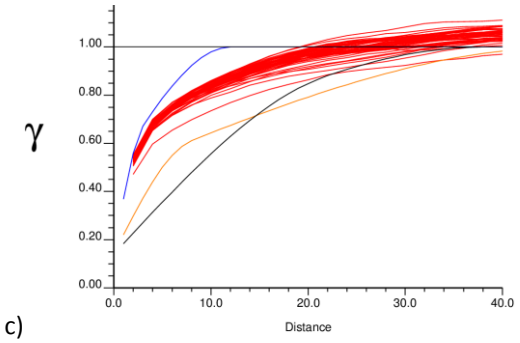

c)

Variograms for gold simulation in diorite

a) Variograms along easting; b) variograms along northing; c) variograms along elevation.

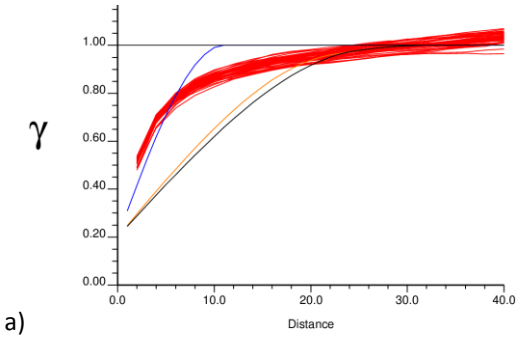

a)

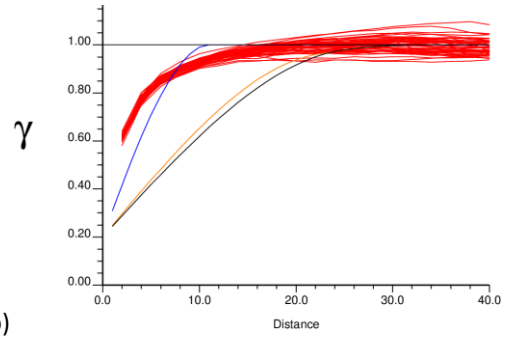

b)

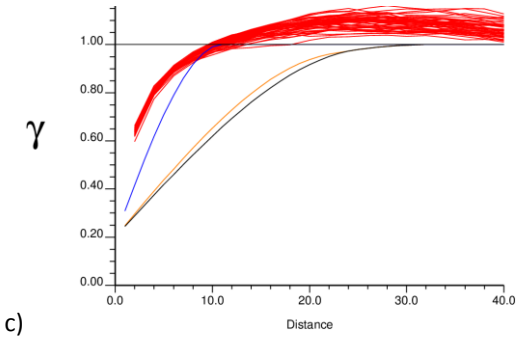

c)

Variograms for gold simulation in quartz-porphyry

a) Variograms along easting; b) variograms along northing; c) variograms along elevation

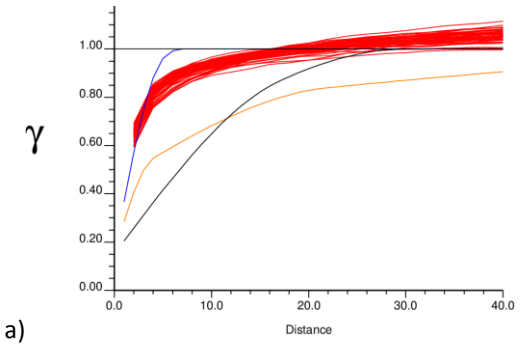

a)

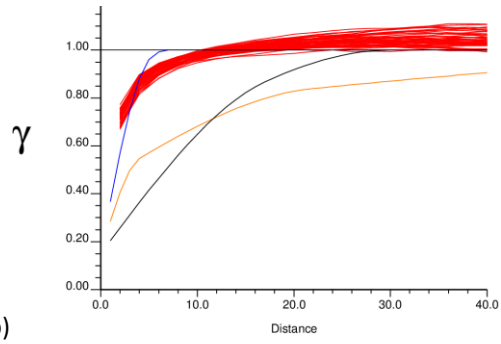

b)

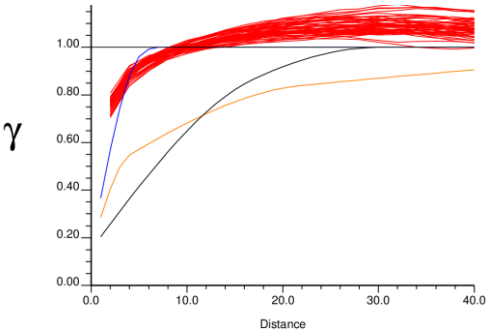

c)